To the Graduate Council:

I am submitting herewith a thesis written by Heather Gastineau entitled " A Test for Oxidation During Metamorphism of L and LL Chondrites." I have examined the final copy of this thesis for form and content and recommend that it be accepted in partial fulfillment of the requirement for the degree of Master of Science, with a major in Geology.

Harry Y. McSween, Jr., Major Professor

We have read this thesis
And recommend its acceptance:

Laurence A. Taylor

Accepted for Council:

Associate Vice Chancellor and
Dean of The Graduate School

A Test for Oxidation During Metamorphism of L and LL Chondrites

A Thesis
Presented for the
Master of Science
Degree
The University of Tennessee

Heather Kay Gastineau
August, 2000

DEDICATION

This thesis is dedicated to my parents,

David and Linda Gastineau

and fiancé

Mitchell Frank Lyons

ACKNOWLEDGEMENTS

I extend my gratitude to all who have contributed to the work of this thesis. First, and for most, my major professor, but more importantly my mentor, Dr. Harry McSween, has given me the patience and guidance to complete this thesis. The help of my committee members Drs. Larry Taylor and Dan Britt have also played a significant role in the quality and understanding of this work and are much appreciated.

Data collection acquired from the electron microprobe was the bulk of my thesis and made a little easier with the patience of Allan Patchen. Without the helpful discussions, provocative questions, and editing assistance, from Rachel Lentz I would not be where I am today. She is one outstanding mentor and best of all, a friend.

The smiles and laughter from Teresa, Denise, and Melody have been a delight while at UT. All three have helped me tremendously in my time of need and made me feel exceptionally welcome in the department.

The friendships made during my stay at UT made each day more enjoyable and have allowed me to keep my sanity the past two years. You all are awesome: Sara Bier, John Collins, Elizabeth Humbert, Dana Miller, Janna Peevler, Pin Promprated, Amy Robinson, Melanie Stewart, Scott Williams, and Michael Wyatt.

I thank the inspiration that were given to me by Drs. Jeffrey Grigsby, Theresa Boundy, and Alan Samuelson from Ball State University and appreciate the strong undergraduate geoscience education they provided. Without their

encouragement, I would not be where I am today. Others at Ball State that I have shared wonderful experiences with are Jessica Barone and Michael Kutis. Their friendships have been a blessing and reminded me to enjoy each day to it's fullest.

Most of all, I thank my family: Mom, Dad, Holly, Aaron, Ethan, Jeanie, and Mitch, for supporting me the past six years of my college education. Your encouragement and love have made me who I am; each of you is a part of me and has a special place in my heart.

ABSTRACT

Subtle but progressive changes in the olivine and low-Ca pyroxene abundances and the olivine, low-Ca pyroxene, and diopside compositions are observed with increasing metamorphic grade in equilibrated (types 4-6) ordinary chondrites. These changes suggest that the meteorites experienced oxidation of metallic Fe during heating according to the reaction:

$$Fe + \frac{1}{2} O_2 + (Mg, Fe)SiO_3 \Rightarrow (Mg, Fe)_2SiO_4$$

metal pyroxene olivine

hypothesized by McSween and Labotka (1993), based on calculated normative mineralogy as well as incorporation of Fe^{2+} into ferromagnesian silicate phases. From this study, two observations support this hypothesis: (1) the modal olivine: low-Ca pyroxene ratio increases with petrologic type in L and LL chondrites and (2) Fe-enrichment in olivine and low-Ca pyroxene are observed from petrologic types 4-6 in the L chondrites. The behavior of the LL chondrites studied is inconsistent; however, a general Fe-enrichment in silicates is apparent.

Characteristic spectral absorption features in visible infrared spectra (VIS-NIR) are sensitive to the olivine/ low-Ca pyroxene abundance ratio and the Ca^{2+} and Fe^{2+} contents of pyroxenes. Therefore, metamorphic grade (petrologic type) in ordinary chondrites might be identified using characteristic spectra since each petrologic type has different olivine/ pyroxene abundances and pyroxene compositions. This work is applicable to the NEAR mission to 433 Eros and other ground-based spectroscopic studies of asteroids.

TABLE OF CONTENTS

LIST OF TABLES

LIST OF FIGURES

1. INTRODUCTION

Ordinary chondrites, the most common types of meteorites that fall to Earth, are samples of asteroids. In addition to revealing otherwise unobtainable information on processes and conditions that occurred within asteroids, the meteorites provide ground truth for the calibration and interpretation of asteroid spectra, the primary means by which these remote bodies are studied.

Metamorphism of ordinary chondrites has been well established; however, whether oxidation or reduction accompanies metamorphism has been debated. Changes in redox state can potentially affect the abundance and composition of minerals in the various petrologic types (metamorphic grades) of chondrites. The purpose of this study is to test the hypothesis that oxidation increases with progressive metamorphism of ordinary chondrites (McSween and Labotka, 1993). Modal mineralogy and mineral chemistry in samples of petrologic types 4, 5, and 6 of the L and LL ordinary chondrites were used to test this hypothesis.

This work has applications to the Near Earth Asteroid Rendezvous (NEAR) mission to 433 Eros and to ground-based spectroscopic studies of asteroids. A goal of the NEAR mission team is to characterize and map the surface mineralogy of 433 Eros using visible-near infrared (VIS-NIR) spectra. Spectral features in the VIS-NIR region are sensitive to silicate mineral abundances and compositions. The surface of Eros is believed to be composed primarily of olivine and pyroxene (Murchie and Pieters, 1996), so it has a mineral assemblage similar to ordinary chondrites. Since reduction or oxidation during metamorphism of ordinary chondrites produce different mineral abundances and

compositions, the results from this study should allow a better interpretation of spectral data from an asteroid surface.

Thermal History of Ordinary Chondrites

Three classes of ordinary chondrites (H, L, and LL) are distinguished by the amount of total and metallic Fe they contain (Keil and Frerikssοn, 1964). Each class is subdivided into four petrologic types ranging from unequilibrated type 3 (most primitive) to equilibrated types 4, 5, and 6 chondrites, reflecting different degrees of thermal metamorphism (Van Schmus and Wood, 1967). In general, equilibrated chondrites are characterized by homogeneous silicate mineral compositions (mainly olivine and low-Ca pyroxene), the presence of sodic plagioclase, and recrystallized textures, whereas unequilibrated chondrites are defined by the presence of igneous glass and heterogenous silicate compositions. Figure 1 illustrates a hypothetical cross-section of an asteroid parent body composed of petrologic types 3, 4, 5, and 6. This 'onion-shell' model postulates that the primitive, petrologic type 3 ordinary chondrites originated on or near the surface of the asteroid, whereas petrologic type 6 material represents the asteroid core region (Dodd, 1969; Anders, 1978; Minster and Allegre, 1979; Pellas and Storzer, 1981). The rapid decay of short-lived radioactive isotopes, especially ^{26}Al, was probably the heat source for the parent body (discussed by Bennett and McSween, 1996). Pyroxene geothermometry suggests petrologic type 6 chondrites experienced peak metamorphic temperatures at ~ 950° C (Dodd, 1981; Harvey et al., 1993). However, the application of the two-pyroxene geothermometer is questionable, because of lack of equilibration of these phases

ASTEROID CROSS-SECTION

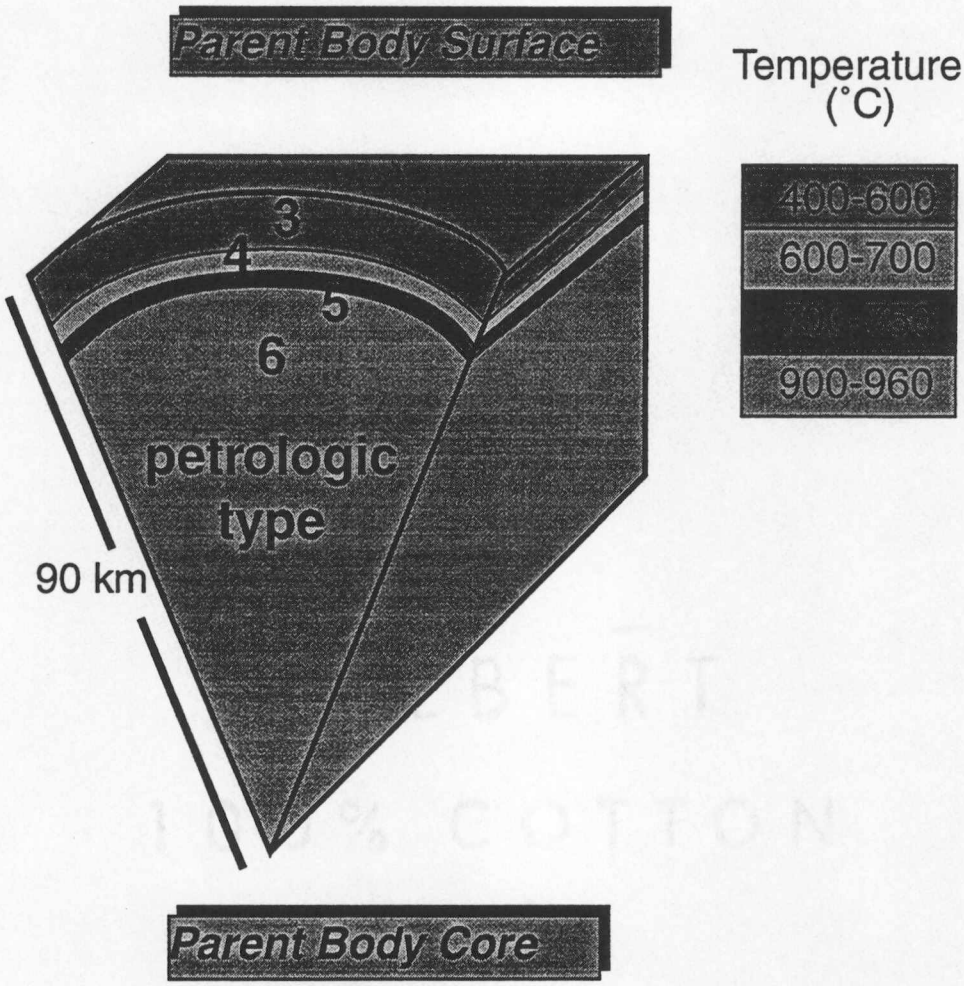

Figure 1: Illustrated here is a cross-sectional view of an asteroid "onion-shell" parent body, composed of petrologic types 3, 4, 5, and 6 after Bennett and McSween (1996). Petrologic type 3 represents the asteroid surface, whereas type 6 represents the asteroid core that experienced peak metamorphic temperatures of 900-960˚C as determined by pyroxene geothermometry.

(McSween and Patchen, 1989). The equilibration temperatures from clinopyroxene compositions alone suggest peak temperatures of 900-960° C for LL6 chondrites (McSween and Patchen, 1989).

Quantitative thermal models developed by Miyamoto et al. (1981) and revised by Bennett and McSween (1996) support the onion-shell structure; however, the onion-shell model is inconsistent with metallographic cooling rates of chondrites (Wood, 1967). To resolve this discrepancy, Scott and Rajan (1981) proposed a rubble-pile structure, a composite body assembled from small, metamorphosed pieces. Davis et al. (1985) suggested that a rubble-pile structure would result from the collision and destruction of onion-shell bodies that later reassembled by gravity. Furthermore, Fe-Ni metallographic cooling rates in the Cangas de Onis H-chondrite breccia vary from 1000 to 1° C per million years and are thought to originate at burial depths from near the surface to 100 km inside the parent body, implying that these parent bodies underwent destruction and reassembly events (Williams et al., 1985).

Reduction vs. Oxidation During Metamorphism of Ordinary Chondrites

Previous research recognized that Fe oxidation state varies among the three ordinary chondrite groups H, L, and LL (Urey and Craig, 1953; Fredriksson et al., 1968; McSween and Patchen, 1989). Superimposed on this trend is a more subtle variation in redox state that appears to relate to metamorphism. However, the nature of this metamorphic variation is controversial.

Dodd (1976) and Sears and Weeks (1986) both observed a bulk Fe-enrichment with metamorphic grade in H, L, and LL chondrites and suggested

that this trend may imply an increase in metallic Fe; however, the bulk chemistry database of ordinary chondrites analyzed by Jarosewich (1990) shows a decrease of metallic Fe with metamorphic grade. The contradiction between the two observations may likely be attributed to the different methods used to obtain metal abundances: Jarosewich (1990) physically separated metal, whereas Sears and Weeks (1986) inferred abundances of metal from concentrations of other siderophile elements in bulk meteorite samples. Dodd (1976) compiled chemistry of ordinary chondrites from wet chemical analyses all prepared since 1950. Interestingly, a previous study by Morgan et al. (1985) also inferred metal abundances from siderophile element abundances and reported a metal decrease from types 4 to 6, supporting Jarosewich's (1990) findings.

Brett and Sato (1984) measured intrinsic oxygen fugacities using a solid-electrolyte oxygen cell on H and LL chondrites and found that an equilibrated chondrite was more reduced than an unequilibrated chondrite of the same class. Brett and Sato (1984) cited two arguments that reduction had occurred during metamorphism of ordinary chondrites: (1) metal in unequilibrated H chondrites contains more Ni than equilibrated H chondrites (Dodd, 1974), and (2) bulk carbon content in ordinary chondrites decreases with increasing metamorphism (Mason, 1979). They used these two lines of evidence to suggest that oxidation of graphite accounted for a small amount of iron reduction in chondrites during metamorphism and with increased metamorphism the remaining carbon dissolved in the metal, thus causing the reduction process to stop because the activity of carbon was lowered.

In addition, Williams (1971a) calculated the oxygen fugacities of types 5 and 6 chondrites using equilibrium constants for various redox reactions in the Fe-Si-O system that he had experimentally determined (Williams, 1971b). His values for the equilibrium constants are greater than those used by Holland and Powell (1990) and Helgeson et al. (1978). Using his experimental values, William's (1971a) calculated oxygen fugacities support the reduction of iron by carbon during metamorphism.

In contrast to those studies, McSween and Labotka (1993) hypothesized that oxidation state increases with progressive metamorphism within each group of ordinary chondrites. The reaction hypothesized to be responsible for the increase in oxidation during chondrite metamorphism is:

$$Fe + \tfrac{1}{2} O_2 + (Mg, Fe)SiO_3 \Rightarrow (Mg, Fe)_2SiO_4$$

metal pyroxene olivine

From this reaction, differences in the relative proportions of olivine, low-Ca pyroxene, and metal in each petrologic type should reflect changes in oxidation state. McSween et al. (1991) estimated mineral abundances in ordinary chondrites by calculating normative mineralogy from measured bulk chemistry of 94 unweathered falls in which metallic Fe and FeS had been measured (Jarosewich, 1990). Results from their work show that the average normative olivine: low-Ca pyroxene ratio increases with petrologic type. Also, McSween and Labotka (1993) observed from the bulk metal analyses of Jarosewich (1990) that the Ni/Fe and Co/Fe ratios of the residual metal increase with petrologic type for each group of chondrites, as would be expected if metallic iron had been

oxidized during metamorphism. Rubin (1990) also noted that Ni and Co contents of kamacite increase with petrologic type in ordinary chondrites.

Other lines of evidence also support oxidation during metamorphism. McSween and Labotka (1993) compiled average H, L, and LL compositional data for olivine and low-Ca pyroxene and found that Fe-enrichment increases with petrologic type. The hypothesized reaction suggests that some of the Fe^{2+} formed by oxidation of metal replaced Mg in olivine and low-Ca pyroxene, in addition to converting some low-Ca pyroxene to olivine. Finally, calculated oxygen fugacities, based on coexisting silicate mineral compositions, increase with petrologic type for H and L chondrites (McSween and Labotka, 1993). For example, the oxygen fugacities (Δ log fO2, relative to the ferrosilite-quartz-iron buffer) for petrologic types 4 to 6 of the L chondrites vary from -1.13 to -1.11, supporting the hypothesis that oxidation of Fe is linked to metamorphic grade of ordinary chondrites.

Therefore, the olivine, low-Ca pyroxene, and metal abundances, coupled with compositional changes of olivine and low-Ca pyroxene and changes in oxygen fugacity, imply that oxidation increases with progressive metamorphism of ordinary chondrites. These lines of evidence contradict the model for chondrite metamorphism involving Fe reduction by graphite.

2. METHODS

Three thin-sections of L chondrites and four thin-sections of LL chondrites, spanning petrologic types 4, 5, and 6, were examined for this study (Table 1). The most desirable chondrite characteristics included low shock grade and unbrecciated samples (see Table 1). Olivenza (LL5) is characterized as a fragmental breccia; however, the two sections used in this study did not appear to contain multiple clasts. All samples chosen, with the exception of Greenwell Springs and Tuxtuac, were identified as 'spectrally clean.' 'Spectrally clean' suggests that the meteorite is not contaminated with terrestrial weathering products, particularly Fe-oxides (Gaffey, 1999). The Fe-oxides create a different spectral effect compared to the spectra acquired from an unweathered sample; consequently, the unweathered meteorites are most useful for calibration. Of the 94 specimens that have calculated normative mineralogy (McSween et al., 1991), 14 have previously measured spectra, and the modal mineral proportions estimated are in fairly good agreement with the normative mineralogy (Gaffey, 1999).

The attempt to choose 'spectrally clean' meteorites was only in case normative differed from modal mineralogy so that after this study, the possibility of a calibration factor could be applied. Nevertheless, the weathering of metal does not affect the olivine: low-Ca pyroxene ratios of chondrites and, therefore, does not interfere with testing the hypothesis that oxidation increases with metamorphism of ordinary chondrites.

TABLE 1. L and LL ordinary chondrites examined in this study.

Chondrite Classification	Name	Spectrally Clean‡	Shock Grade	Collection
L4	Bald Mountain	Y	S4[3]	USNM 851-1
L5	Homestead	Y	S3[3]	USNM 423
L6	Girgenti	Y	S4[1]	USNM 1453-1
LL4	Greenwell Springs		S3[1]	USNM 6379-2
LL5	Olivenza (1)	Y	S3[2*]	USNM 5955-1
LL5	Olivenza (2)	Y	S3[2*]	H. McSween
LL5	Tuxtuac		S4[1]	Field ME 2850 No. 4
LL6	Saint Severin	Y	S3[1]	USNM 2608-3

‡ Gaffey (1999)

Sources for shock classification

1 this work
2 Stöffler et al. (1991)
3 Rubin (1993)

* Fragmental breccia

Modal Mineralogy

Despite extensive study of the ordinary chondrites, modal mineralogy data sets do not exist. The fine-grained nature of these chondrites is problematic for optical point-counting methods, and it is often difficult to distinguish silicate phases. Electron microprobe compositional mapping is an alternative to the traditional petrographic point-counting method. The modal abundances of minerals using the *Feature Scan* microanalysis technique were obtained with an Oxford Instruments (LINK) Model eXL II energy dispersive spectrometer (EDS) mounted on a Cameca SX-50 electron microprobe at the University of Tennessee. Preliminary work was done, using the EDS, to determine the measured elements in the various phases of interest within a sample. *Feature Scan* then allows user-defined windows to identify the phases present in a sample (Taylor et al., 1996). For example, specific ranges of Si, Ca, and Mg contents are used to identify olivine. Table 2 lists the X-ray spectral criteria used to classify the various mineral and glass phases present in the meteorites for this study. The conditions are set for the acquisition of X-ray data by the EDS, including the excitation potential (20 kV), beam current (3 nA), dwell (counting) time (40-60 sec), and sampling mode (whole particle, 1 μm beam size).

Feature Scan is a semi-quantitative technique with an estimated precision of ~ 5% of the amount of each mineral present (Taylor et al., 1996). An EDS spectrum was acquired at every 4th pixel (step size ~ 16 μm). A back scatter electron (BSE) image in Figure 2 illustrates the *Feature Scan* technique. The total number of points analyzed varied from ~ 10,000 to ~ 80,000 per thin-section

TABLE 2. X-ray spectral criteria used to classify minerals and glass phases. †

Phase*	Defining Criteria ‡
olivine	36-55% Si, 18-55% Mg, and 0-2% Ca
low-Ca pyroxene	55-70% Si, 13-30% Mg, and 0-3% Ca
plagioclase	50-75% Si and 12-35% Al
diopside	45-70% Si, 5-20% Mg, 15-35% Ca, and 0-4% Al
pigeonite	55-70% Si, 12-25% Mg, and 3-12% Ca
troilite	> 20% S
taenite	55-90% Fe and >20% Ni
kamacite	> 80% Fe and > 10% Ni
chromite	> 20% Cr
ilmenite	> 40% Ti
whitlockite	> 10% P and > 20% Ca
K-rich glass	> 5% K
silica phase	38-66% Si and 4-15% Al

† These criteria are only applicable to identify phases in the L and LL meteorites of this study.

‡ These criteria are in terms of percentage of spectrum as provided by the *Feature Scan* X-ray imaging software. The values are similar to the oxide weight percentages for given elements.

* The minerals and glasses are arranged in the order in which they are tested for fit. For example, the EDS spectrum acquired does not meet the olivine criteria so it is then tested for low-Ca pyroxene, etc.

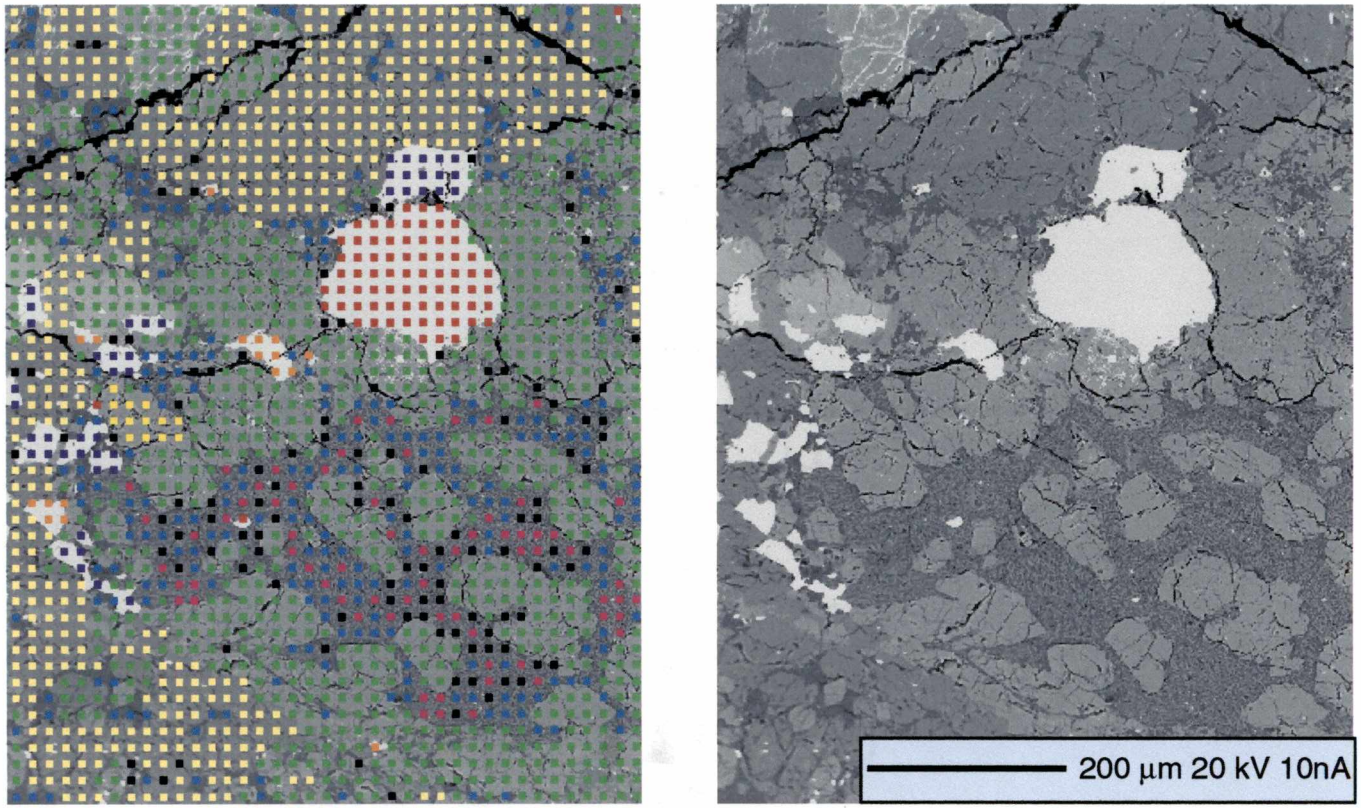

Figure 5: Shown above is a back scatter electron image (BSE) of the L5 chondrite Homestead. On the left, the BSE image is superimposed with colored blocks indicating the location at which an energy dispersive spectrum (EDS) analysis was taken at every 16th µm using the *Feature Scan* technique. The EDS analysis is then matched according to its appropriate mineral phase counterpart. Mineral phases correspond to the following colors: olivine, green; orthopyroxene, yellow; plagioclase, blue; troilite, red; taenite, purple; kamacite, orange; silica phase, pink; and unclassified, black. On the right is the same image as shown on the left; however, the blocks were eliminated to illustrate the varying shades of gray which are classified by the BSE. The more brightly illuminated colors (white) reflect higher Fe contents.

(see Table A1 in Appendix A), significantly more than in conventional optical point-counting. EDS spectra that do not meet the defined mineral criteria are determined 'unclassified', and most likely represent grain boundaries and unidentified phases. All phases are renormalized to 100% after the unclassified (average ~ 8% in each meteorite) is subtracted from the total (described in Table A2 of Appendix A). Renormalizing to 100% is equivalent to distributing the unclassified proportionally among each phase present.

The modes that *Feature Scan* produces are given as area %. In this study, the modal mineralogy is compared to normative mineralogy, so it is necessary to convert the modal mineralogy produced by *Feature Scan* (area %, assumed to equal volume %) to weight % (Table A3-A10). The density of each phase is needed for this calculation (see Table A2).

Quantitative Chemical Analyses

Compositional data have been obtained for four individual grains of olivine, low-Ca pyroxene, and diopside in meteorites of petrologic types 5 and 6. Four grains of olivine and diopside and seven grains of low-Ca pyroxene were analyzed in meteorites of petrologic type 4. A minimum of two core and rim analyses were analyzed for each grain, although in some cases more analyses were accomplished.

Major element compositions were determined by electron microprobe using the four-spectrometer Cameca SX-50. The accelerating voltage was 15 kV with a beam current of 30 nA. The beam size was 1 μm and counting times of 20 seconds were used for all elements. All data were corrected using ZAF

procedures incorporated in the Cameca software. Analyses are presented in Appendix B.

3. RESULTS

Modal Mineralogy

The modal weight % abundances obtained by recalculating *Feature Scan* data for the meteorites in this study are listed in Table 3. Figures 3a and b compare the modal and normative olivine: low-Ca pyroxene ratios for L and LL chondrites, respectively. As previously mentioned, the normative olivine: low-Ca pyroxene ratio increases with petrologic type for L and LL chondrites. The modal ratio for the L chondrites increases with petrologic type and the trend mimics that of the normative ratio calculated for the same chondrites; however, the mode is offset consistently to lower values in comparison to the norm. The modal olivine: low-Ca pyroxene ratio for the LL chondrites also increases with petrologic type and is lower compared to the norm, although its offset is inconsistent with the norm for the LL5 chondrite. I am confident in the olivine: low-Ca pyroxene modal ratio for petrologic type 5, since two different sections of Olivenza (LL5) and one section of Tuxtuac (LL5) all have similar ratios.

The modal mineralogy reveals several other interesting observations in comparison to the norm. The diopside and plagioclase modal abundances in L (Fig. 4a, b) and LL (Fig. 4c, d) chondrites increase with petrologic type. The modal abundance of these two phases disagree with those reported in the norm, as well as those of metal and troilite compared to the amounts determined by bulk chemistry (Jarosewich, 1990). In addition, the presence of a silica phase

TABLE 3. Modal abundances for L and LL chondrites.

Phase	Meteorite							
	Bald Mountain (L4)	Homestead (L5)	Girgenti (L6)	Greenwell Springs (LL4)	Olivenza (LL5) (section 1)	Olivenza (LL5) (section 2)	Tuxtuac (LL5)	Saint Sevrin (LL6)
silica phase	5.74	5.47	N. A.	6.65	4.69	3.01	3.92	N. A.
K-rich glass	0.06	0.04	N. A.	0.29	0.17	0.13	0.20	N. A.
whitlockite	0.60	0 41	0.58	0.73	0.75	0.47	0.42	0.34
ilmenite	0.00	0.00	0.00	0.00	0.00	0.01	0.05	0.00
chromite	0.67	0.73	1.00	0.91	1.15	0.81	1.01	1.06
kamacite	7 64	11.01	4.00	0.73	0 10	0 24	0.10	0.56
taenite	1 58	1.44	2.03	1.52	1.68	3.23	2.59	1.26
troilite	8.08	6.56	8.36	7.67	5.16	5.62	7.65	6.16
pigeonite	6.81	3 92	1.68	4.96	2.93	1.76	2.59	1.61
diopside	1.95	2.19	5.15	2.66	3.91	3.33	4.70	5.47
plagioclase	5.66	6 45	9.55	7 83	10.01	10.87	9.23	10.50
low-Ca pyroxene	26.97	26.78	26.09	22.99	19.29	21.25	19 21	20.87
olivine	34 23	34.98	41.57	43.06	50.17	49.26	48.34	52.19
Total	100 00	100.00	100.00	100.00	100.00	100.00	100.00	100.00

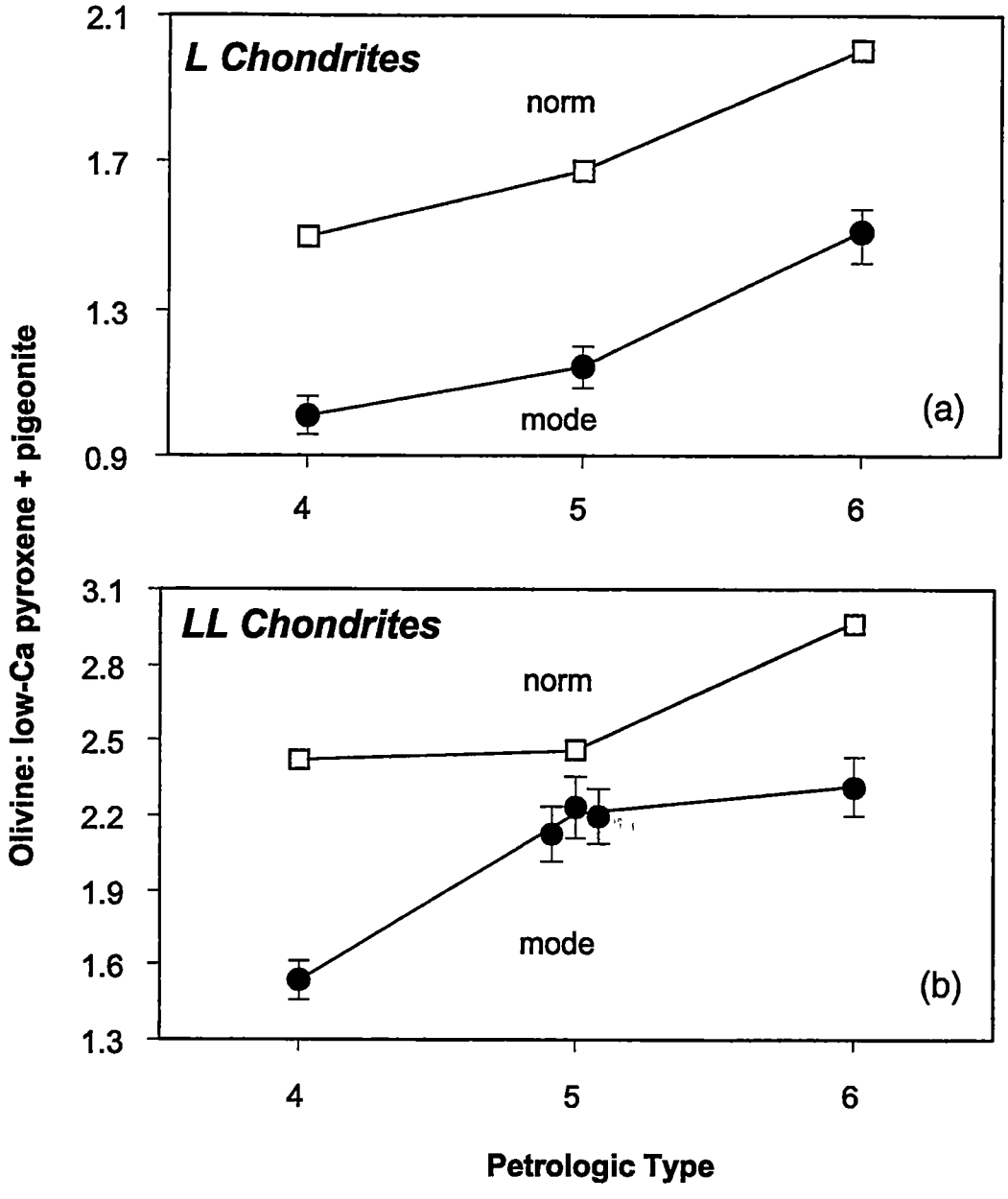

Figure 3: The normative and modal olivine: low-Ca pyroxene ratio increases with petrologic types 4, 5, and 6 in L (a) and LL (b) chondrites; however, the mode ratio is offset from the norm. The error determining the modal mineralogy from *Feature Scan* is about 5 % relative of the phase present.

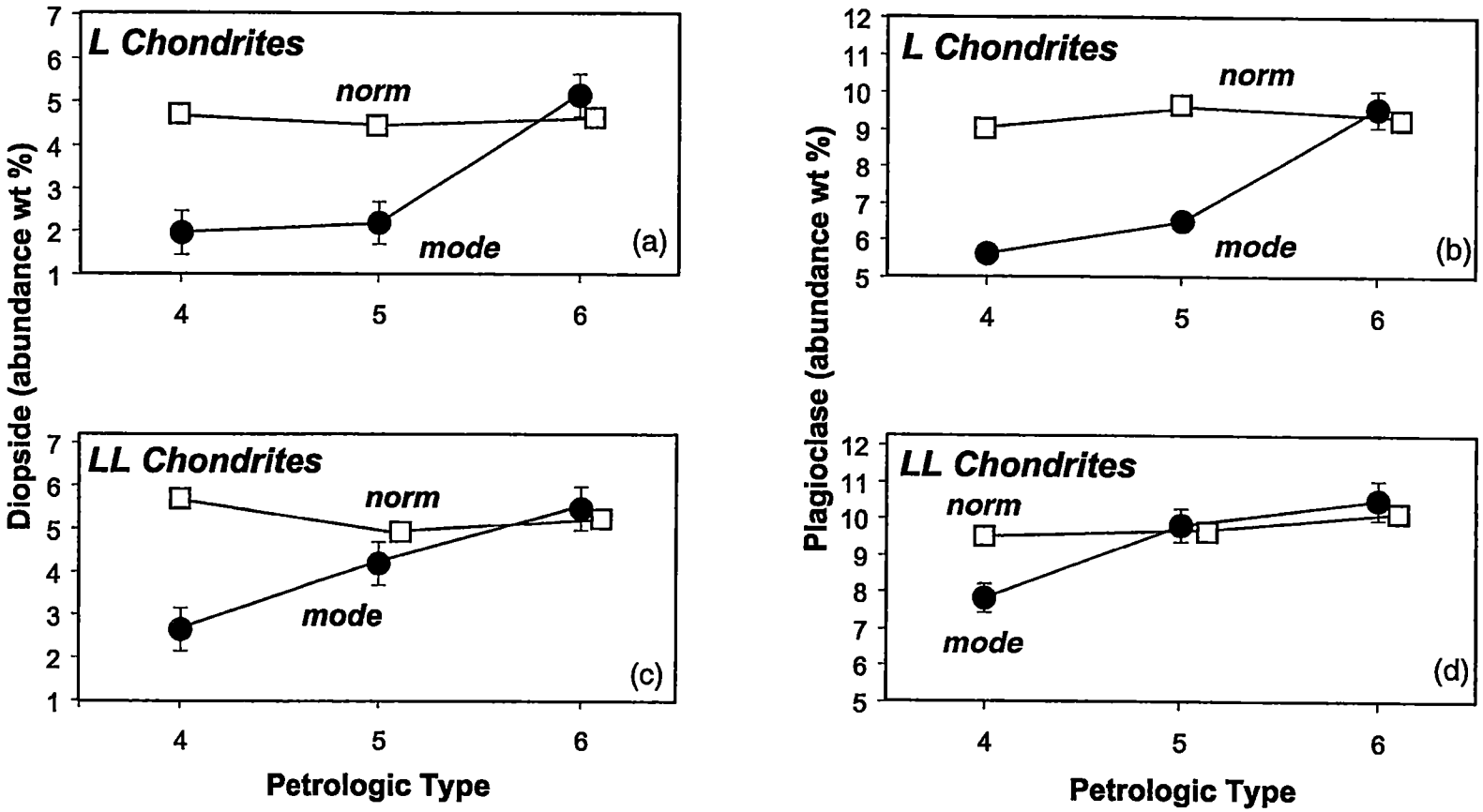

Figure 4: The diopside and plagioclase modal abundances increase with petrologic type in L (a, b) and LL chondrites (c, d). These modes disagree with the calculated norms, except for type 6 chondrites (McSween et al., 1990).

4-6%) was observed in each of the ordinary chondrites studied and is texturally intergrown with plagioclase (Fig. 5).

Quantitative Chemical Analyses

The results of the average electron microprobe analyses for olivine, low-Ca pyroxene, and diopside are shown in Tables 4, 5, and 6, respectively, for each of the L and LL chondrites in this study. The grain compositions used to obtain averages are compiled for each chondrite in Appendix B.

Goodrich and Delaney (1999) constructed a plot organizing all chondrites according to their molar Fe/Mn and Fe/Mg ratios. From this, they re-emphasized that LL chondrites are more oxidized compared to H chondrites. Rather than plotting a bulk average for the L and LL chondrite data acquired, I have chosen to plot the molar Fe/Mn and Fe/Mg ratios for olivine, low-Ca pyroxene, and diopside of petrologic types 4, 5, and 6. The molar Fe/Mn and Fe/Mg for olivine and low-Ca pyroxene increase from petrologic types 4 to 6 within the L chondrites, whereas diopside shows an Fe-enrichment from type 4 to 6 with the exception of type 5 (Fig. 6). Interestingly, the molar Fe/Mn and Fe/Mg ratios for diopside of LL chondrites increase with petrologic type; however, the low-Ca pyroxene and olivine of petrologic type 5 have higher ratios compared to type 6 (Fig. 7). Electron microprobe data of L and LL chondrites have been collected from the literature and plotted on the appropriate molar Fe/Mn and Fe/Mg figures and therefore, envelopes (fields) illustrate the variability of the Fe/Mn and Fe/Mg ratios of olivine, low-Ca pyroxene, and diopside of the different petrologic types for L and LL chondrites.

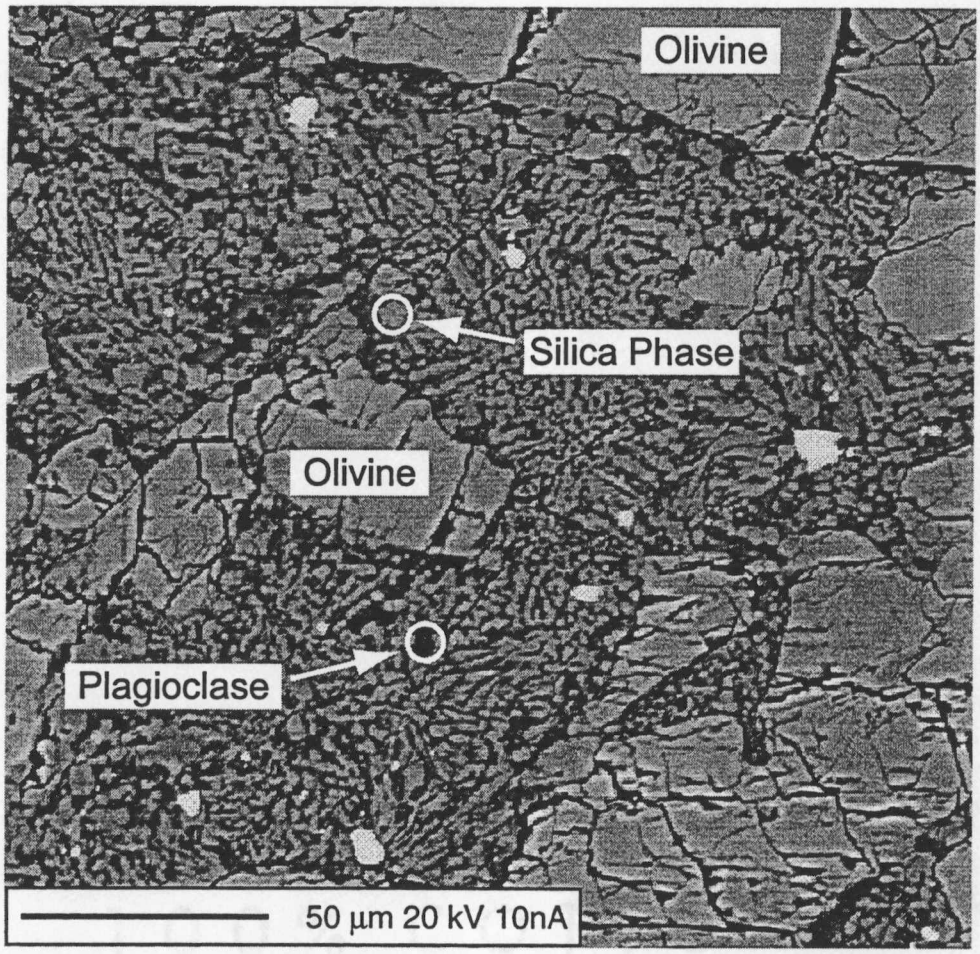

Figure 5: The plagioclase and silica phase are displayed in the BSE image of the L5 chondrite Homestead and are texturally intergrown with each other. The silica phase also coexists with olivine.

TABLE 4. Average electron microprobe analyses for olivine of each L and LL chondrites.

	GL6 [16]	HL5 [16]	BML4 [24]	SSLL6 [16]	OLL5 [32]	TLL5 [16]	GWLL4 [24]
SiO_2	38.3 (1)*	37.9 (2)	38.2 (2)	37.6 (6)	37.1 (2)	37.2 (1)	36.8 (2)
TiO_2	< 0.03	< 0.03	< 0.03	< 0.03	< 0.03	< 0.03	< 0.03
Al_2O_3	< 0.03	< 0.03	< 0.03	< 0.03	< 0.03	< 0.03	< 0.03
Cr_2O_3	< 0.03	< 0.03	< 0.03	0.03 (2)	0.03 (2)	0.03 (2)	< 0.03
MgO	38.9 (2)	39.5 (2)	40.1 (1)	35.5 (1)	35.2 (1)	35.0 (0)	36.5 (1)
CaO	< 0.03	0.03 (0)	< 0.03	0.04 (1)	0.04 (1)	< 0.03	< 0.03
MnO	0.44 (1)	0.45 (2)	0.46 (2)	0.44 (1)	0.44 (2)	0.44 (0)	0.46 (2)
FeO	22.9 (0)	21.5 (9)	21.2 (1)	26.1 (3)	26.8 (2)	27.5 (2)	25.6 (1)
Na_2O	< 0.03	< 0.03	< 0.03	< 0.03	< 0.03	< 0.03	< 0.03
Total	100.50	99.40	99.98	99.71	99.67	100.22	99.37
Cations based on 4 oxygens							
Si	0.994	0.989	0.990	1.000	0.993	0.991	0.982
Ti	0.000	0.000	0.000	0.000	0.000	0.001	0.000
Al	0.000	0.000	0.000	0.000	0.001	0.000	0.000
Cr	0.000	0.000	0.001	0.001	0.001	0.001	0.000
Mg	1.505	1.538	1.548	1.407	1.403	1.392	1.454
Ca	0.000	0.001	0.001	0.001	0.001	0.001	0.001
Mn	0.010	0.010	0.010	0.010	0.010	0.010	0.010
Fe	0.496	0.471	0.459	0.580	0.599	0.613	0.571
Na	0.000	0.000	0.001	0.000	0.001	0.000	0.000
Total	3.006	3.010	3.009	2.999	3.007	3.008	3.018
Fe/Mn	50.9	47.7	45.5	58.6	61.2	61.3	55.2
Fe/Mg	0.33	0.31	0.30	0.41	0.43	0.44	0.39

G: Girgenti, H: Homestead, BM: Bald Mountain, SS: Saint Severin, O: Olivenza, T: Tuxtuac, and GW: Greenwell Springs

* The number in parentheses represents the one sigma precision of replicate analyses as expressed by the least digit cited.

TABLE 5. Average electron microprobe analyses for low-Ca pyroxene of each L and LL chondrite.

	GLL6 [23]	HL5 [16]	BML4 [48]	SSLL6 [16]	OLL5 [32]	TLL5 [16]	GSLL4 [42]
SiO_2	55.3 (3)*	55.2 (4)	55.9 (2)	55.1 (1)	54.5 (2)	54.7 (1)	54.9 (3)
TiO_2	0.19 (3)	0.13 (4)	0.12 (5)	0.20 (3)	0.15 (4)	0.14 (3)	0.11 (3)
Al_2O_3	0.16 (2)	0.23 (21)	0.15 (7)	0.17 (1)	0.18 (12)	0.11 (2)	0.20 (9)
Cr_2O_3	0.12 (1)	0.19 (13)	0.12 (5)	0.15 (5)	0.14 (8)	0.07 (2)	0.17 (12)
MgO	29.1 (2)	29.5 (4)	30.0 (2)	27.2 (1)	27.3 (1)	27.2 (1)	28.0 (3)
CaO	0.81 (5)	0.65 (28)	0.43 (17)	0.88 (4)	0.80 (7)	0.72 (3)	0.51 (14)
MnO	0.47 (2)	0.46 (3)	0.46 (1)	0.44 (1)	0.44 (1)	0.45 (1)	0.44 (3)
FeO	13.9 (1)	13.3 (2)	13.0 (1)	15.8 (1)	15.8 (2)	16.4 (10)	15.4 (2)
Na_2O	< 0.03	< 0.03	< 0.03	< 0.03	< 0.03	< 0.03	< 0.03
Total	99.99	99.67	100.23	99.94	99.32	99.78	99.67
Cations based on 4 oxygens							
Si	1.980	1.978	1.987	1.992	1.983	1.985	1.984
Ti	0.005	0.003	0.003	0.005	0.004	0.004	0.003
Al	0.006	0.010	0.006	0.007	0.008	0.004	0.008
Cr	0.003	0.012	0.004	0.004	0.004	0.002	0.005
Mg	1.552	1.575	1.587	1.463	1.482	1.474	1.508
Ca	0.031	0.025	0.016	0.034	0.031	0.028	0.020
Mn	0.014	0.014	0.014	0.013	0.013	0.014	0.013
Fe	0.417	0.399	0.387	0.477	0.481	0.497	0.465
Na	0.001	0.001	0.001	0.001	0.002	0.001	0.001
Total	4.010	4.011	4.005	3.998	4.008	4.008	4.007
Fe/Mn	29.2	28.7	28.1	35.4	35.9	35.8	34.6
Fe/Mg	0.27	0.25	0.24	0.33	0.32	0.34	0.31

G: Girgenti, H. Homestead, BM: Bald Mountain, SS: Saint Severin, O: Olivenza, T: Tuxtuac, and GW: Greenwell Springs

* The number in parentheses represents the one sigma precision of replicate analyses as expressed by the least digit cited.

TABLE 6. Average electron microprobe analyses for diopside of each L and LL chondrite.

	GLL6 [23]	HL5 [13]	BML4 [17]	SSLL6 [24]	OLL5 [16]	TLL6 [16]	GSLL4 [17]
SiO_2	53.9 (1)*	53.8 (2)	53.9 (3)	53.2 (2)	53.6 (3)	53.7 (1)	53.2 (3)
TiO_2	0.46 (1)	0.29 (9)	0.33 (5)	0.43 (1)	0.38 (5)	0.35 (2)	0.41 (8)
Al_2O_3	0.49 (2)	0.46 (3)	0.53 (15)	0.49 (1)	0.47 (4)	0.40 (2)	0.97 (30)
Cr_2O_3	0.79 (6)	0.80 (4)	1.18 (44)	0.78 (2)	0.70 (3)	0.69 (4)	0.97 (20)
MgO	16.7 (2)	16.8 (2)	17.6 (7)	16.1 (2)	16.4 (3)	16 2 (1)	16.9 (2)
CaO	21.7 (3)	22.1 (3)	20.1 (26)	21.4 (2)	21.4 (2)	22.0 (2)	20.4 (1)
MnO	0.23 (1)	0.20 (2)	0.30 (9)	0.23 (1)	0.22 (1)	0.20 (2)	0.24 (3)
FeO	4.79 (11)	4.19 (12)	4.80 (1.11)	6.03 (29)	5.65 (7)	5.56 (26)	5.53 (21)
Na_2O	0.54 (2)	0.56 (3)	0.65 (11)	0.51 (2)	0.49 (1)	0.46 (2)	0.50 (4)
Total	99.66	99.24	99.36	99.13	99.29	99.55	99.12
Cations based on 4 oxygens							
Si	1.982	1.983	1.978	1.977	1.983	1.984	1.967
Ti	0.013	0.008	0.009	0.012	0.011	0.010	0.011
Al	0.021	0.020	0.023	0.021	0.021	0.018	0.042
Cr	0.023	0.024	0.034	0.023	0.020	0.020	0.028
Mg	0.915	0.923	0.967	0.890	0.903	0.892	0.931
Ca	0.857	0.874	0.793	0.852	0.850	0.870	0.809
Mn	0.007	0.006	0.009	0.007	0.007	0.006	0.008
Fe	0.147	0.129	0.148	0.187	0.175	0.172	0.171
Na	0.038	0.040	0.046	0.037	0.035	0.033	0.036
Total	4.002	4.007	4.007	4.007	4.004	4.004	4.004
Fe/Mn	20.4	20.5	15.9	26.6	26.1	28.3	22.5
Fe/Mg	0.16	0.14	0.15	0.21	0.19	0.19	0.18

G: Girgenti, H: Homestead, BM: Bald Mountain, SS: Saint Severin, O: Olivenza, T: Tuxtuac, and GW: Greenwell Springs

* The number in parentheses represents the one sigma precision of replicate analyses as expressed by the least digit cited.

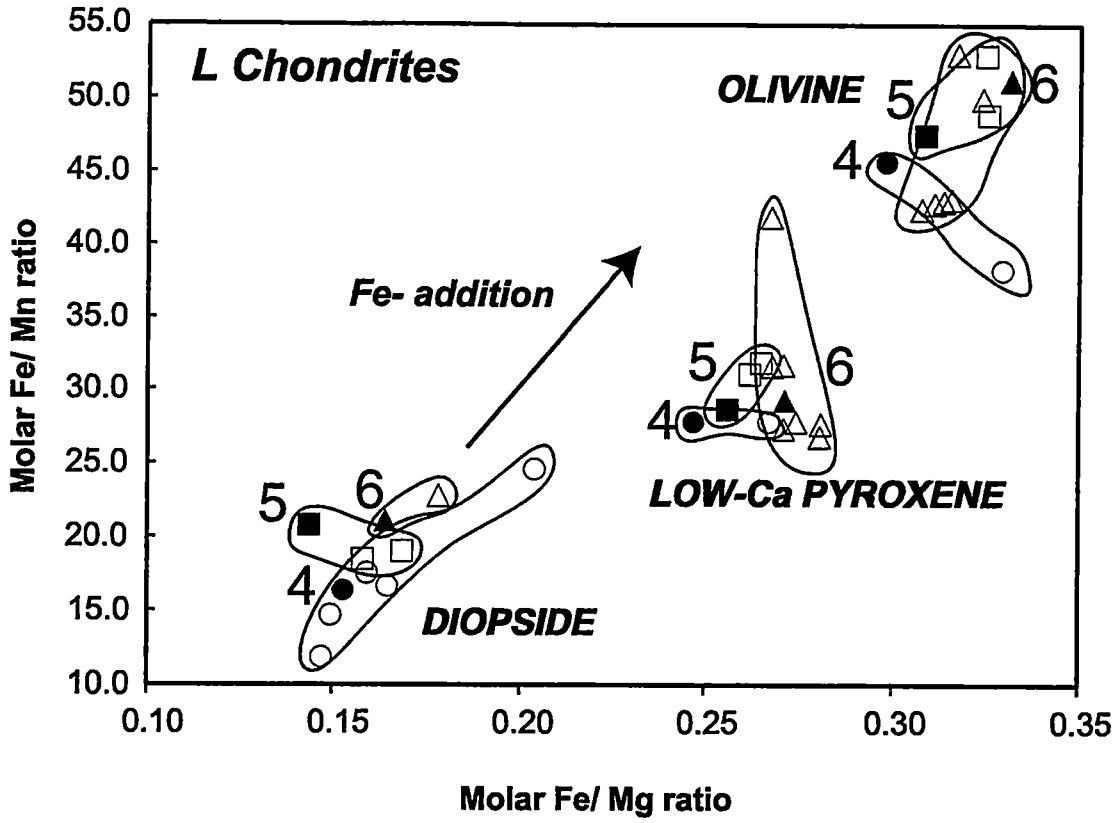

Figure 6: Envelopes outline the Fe/Mn and Fe/Mg molar ratios of olivine, low-Ca pyroxene, and diopside of petrologic types 4, 5, and 6 for L chondrites. Solid symbols represent data collected in this study; circles: type 4, squares: type 5, and triangles: type 6. One standard deviation error on the data collected for this study is less than the size of the symbol. Clearly, an Fe-enrichment is observed in low-Ca pyroxene and olivine with petrologic type, whereas this is not apparent in diopside. Sources of previously published electron microprobe data, shown as open symbols, are as follows: Berkley et al. (1978), Baryshnikova et al. (1985), Dodd and Jarosewich (1981), Keil et al. (1978), Lange et al. (1973), Scorzelli et al. (1998), Shervais et al. (1986), and Smith et al. (1972). The petrologic type fields created using other data from the literature do overlap one another; however, a general Fe-enrichment occurs with petrologic type, suggesting that oxidation increases with progressive metamorphism.

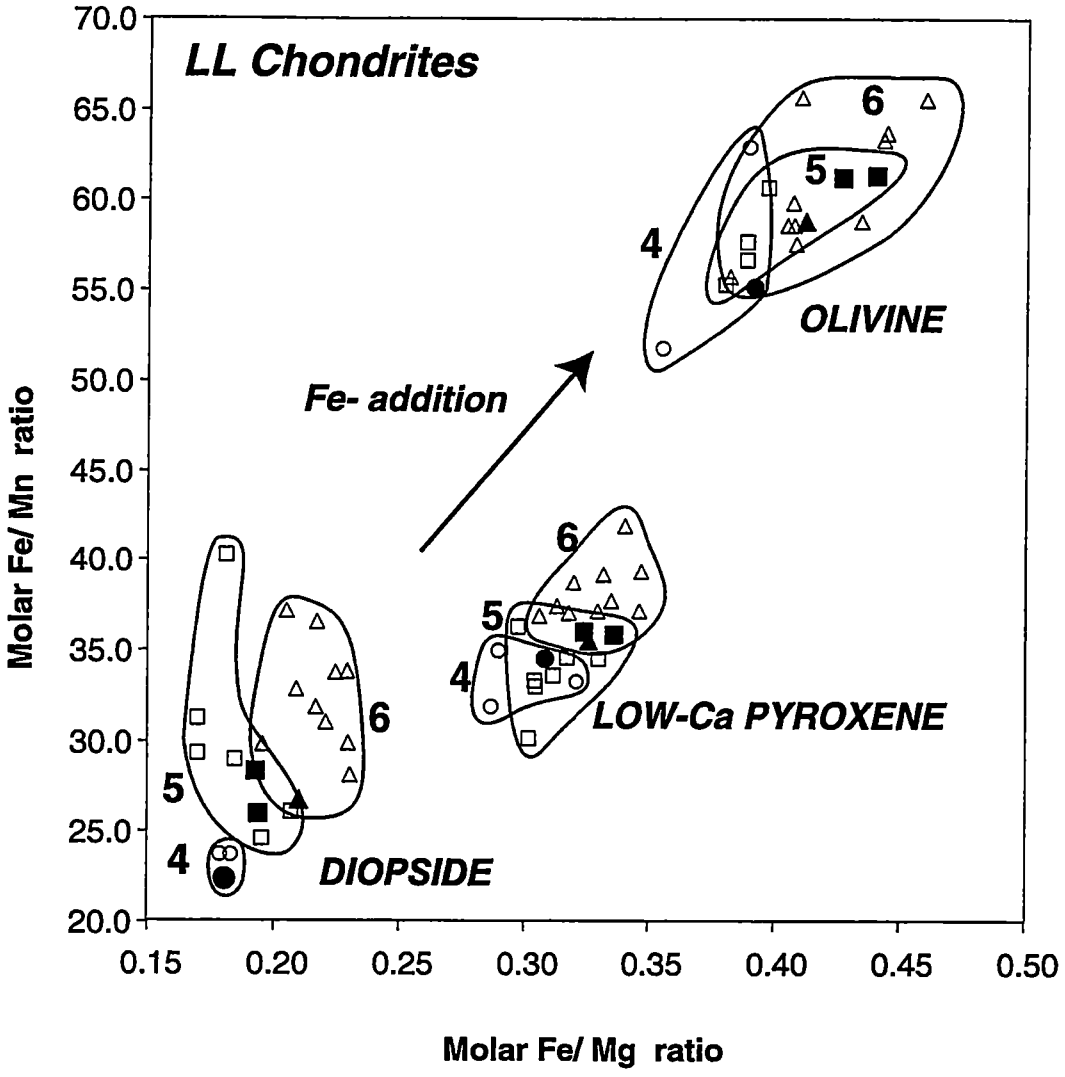

Figure 7: The Fe/Mn and Fe/Mg ratios are plotted for olivine, low-Ca pyroxene, and diopside of each petrologic type for the LL chondrites. Solid symbols indicate data collected from this research: circles: type 4, squares: type 5, and triangles: type 6. One standard deviation error on the data collected for this study is less than the size of the symbol. An Fe-enrichment is observed in diopside from types 4 to 6, whereas type 5 has a higher Fe/Mn and Fe/Mg ratio compared to type 6 for olivine and low-Ca pyroxene. Other sources of electron microprobe data, shown as open symbols, were collected from the the following: Heyse (1978), McSween and Patchen (1989), and Sighinolfi et al. (1991). The fields created for each petrologic type with literature data overlap one another as the L chondrites except for diopside.

Despite trends in major elements, minor oxides are also affected by petrologic type and behave identically within low-Ca pyroxene and diopside of L and LL chondrites. The CaO wt. % content increases from petrologic types 4 to 6 within low-Ca pyroxene (Fig. 8a), whereas it decreases from types 5 to 6 in diopside (Fig. 8b). The TiO_2 wt. % content increases from types 5 to 6 within low-Ca pyroxene and diopside (Fig. 8c, d). On the other hand, the minor oxides Al_2O_3 and Cr_2O_3 do not vary consistently with petrologic type. All minor oxides in olivine, with the exception of MnO, were at or below the detection limit and are insignificant for the purposes of this study.

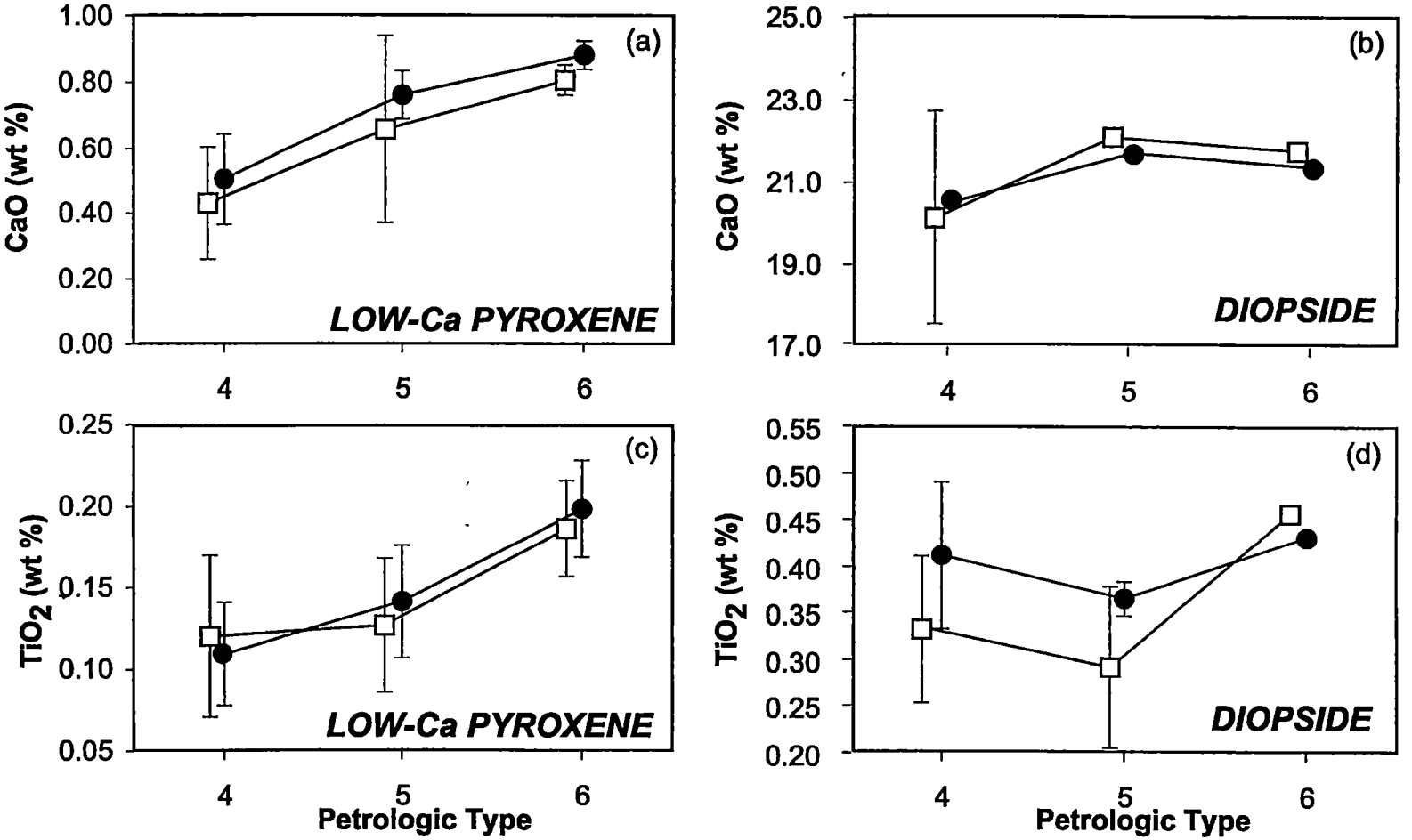

Figure 8: Circles represent L chondrites and squares represent LL chondrites. The CaO wt. % content increases in low-Ca pyroxene with petrologic type (a) and decreases from types 5 to 6 in diopside (b) within L and LL chondrites. The TiO_2 wt. % content in low-Ca pyroxene and diopside increases from types 5 to 6 in L and LL chondrtes (c, d). Error bars show one standard deviation or in some cases plot within the symbol.

4. DISCUSSION

Modal and Normative Mineral Abundances

According to the hypothesized oxidation reaction during metamorphism, the iron from metal oxidation diffuses into silicate minerals and, thus, is converted into olivine. Therefore, the olivine abundance increases at the expense of low-Ca pyroxene, so an increase in the olivine: low-Ca pyroxene ratio with petrologic type reflects an increase in oxidation state. This study provides evidence that the modal olivine: low-Ca pyroxene ratio does indeed increase with petrologic type as do normative ratios (McSween et al., 1990), supporting the hypothesis that oxidation increases with progressive metamorphism of L and LL chondrites.

Despite searches for textural evidence demonstrating the frozen redox reaction, none were found. Metal and low-Ca pyroxene grain boundaries with the presence of selvage olivine are the most likely location to find this textural evidence supporting the frozen reaction. In addition, there was no chemical variation of iron observed in large olivine and low-Ca pyroxene grains located near or far from metal. Perhaps, textural evidence supporting the redox reaction may lie within silicate minerals in the fine-grained matrix.

Mode and Norm Discrepancy

Sample bias is possibly a factor contributing to the difference between the modal and normative olivine: low-Ca pyroxene ratios and other mineral abundances such as diopside, plagioclase, metal, and troilite. Jarosewich (1990) determined the metal and troilite abundances of meteorites and emphasized the importance of sample size in determining accurate abundances. Thin-sections

naturally introduce sample bias to the study. Since metal is heterogeneously distributed throughout the meteorite, one thin-section may contain more metal than another, depending on the cut that was taken from the meteorite. Sample bias might explain the difference in mode and norm abundances, but the consistency in offsets between the mode and norm may suggest otherwise.

Alternative ideas may explain the discrepancy between the modal and normative olivine: low-Ca pyroxene ratio. The norm is designed to calculate the mineralogy of terrestrial rocks and, therefore, may have difficulty in dealing with extremely reduced, metal-bearing rocks such as ordinary chondrites. The calculated chemical compositions of normative olivine and pyroxene disagree with actual measured mineral compositions in H, L, and LL chondrites (McSween et al., 1991), because the Fe/Mg distribution coefficient between normative olivine and hypersthene is not the same as that measured in coexisting phases of experimental charges (Madaris, 1969).

Finally, I considered the possibility that the presence of the silica phase might be responsible for the difference between the mode and norm. However, if this silica phase was responsible, the modal olivine: low-Ca pyroxene ratio would be higher relative to the norm (opposite to what is observed), because the norm uses the excess silica to produce more pyroxene at the expense of olivine.

Van Schmus and Wood (1967) use the presence of chondrule glass as a criterion to identify the various petrologic types of the ordinary chondrites. They found glass present only in unmetamorphosed and slightly-metamorphosed chondrites (types 3 and 4). During metamorphism, the glass crystallizes to

plagioclase and it has been generally believed that plagioclase formation was complete before type 5 metamoprhic conditions. However, this study shows that the increasing modal plagioclase abundance does not converge with the calculated normative plagioclase abundance until type 6 in L and LL chondrites (Fig. 4b, d). The increase in the modal plagioclase abundance from petrologic types 5 to 6 suggests that glass is present in type 5 chondrites and is converted into plagioclase during metamorphism.

Fe/Mn and Fe/Mg Test for Oxidation of Metal

The hypothesized oxidation reaction also suggests that as metal is oxidized during metamorphism of chondrites, the Fe^{2+} diffuses into the silicate minerals, resulting in an Fe-enrichment of olivine and low-Ca pyroxene.

Increases in the molar Fe/Mn and Fe/Mg ratios with petrologic type reflect an increase in redox state. The fields established for the different petrologic types, based on my data and that from the literature, clearly indicate a general Fe-enrichment (relative to Mn and Mg) in olivine, low-Ca pyroxene, and diopside from petrologic types 4-6 (Figs. 6, 7), supporting oxidation increase with progressive metamorphism of ordinary chondrites. However, the fields overlap somewhat. The boundaries between petrologic types are arbitrary breaks within a gradational sequence. Thus, chondrites of the same petrologic type may have experienced different peak metamorphic temperatures, and the temperature difference for chondrites of different types might be relatively small. For example, one type 5 chondrite may have been exposed to temperatures close to

a type 6, whereas another type 5 may have experience temperatures similar to type 4.

Equilibrium Among Phases

Ordinary chondrites have been subjected to intense heat during metamorphism, causing the homogenization of olivine, low-Ca pyroxene, and diopside compositions. Tie lines connecting olivine and diopside to low-Ca pyroxene of the same petrologic type can be used to test if these phases reached equilibrium with one another or retained equilibrium during cooling in terms of molar Fe/Mn and Fe/Mg. The tie lines from my data for L chondrites do not intersect between olivine and low-Ca pyroxene (Fig. 9a), whereas they cross in the LL chondrites (Fig. 10a), and all tie lines intersect between diopside and low-Ca pyroxene (Figs. 9b and 10b) in both chondrite types. The tie lines connecting data from the literature are roughly parallel and appear to approach equilibrium; however, the fact remains that they also intersect.

Several reasons may be responsible for the intersection of tie lines between phases from my data and the literature. As stated prior, the boundaries between petrologic types are arbitrarily defined and the actual sequence is gradational. On the other hand, olivine, low-Ca pyroxene, and diopside may have reached equilibrium at peak metamorphic temperatures; however, during cooling the diffusion of Fe and Mg in olivine continued to a lower temperature compared to low-Ca pyroxene and diopside. In contrast to this, it is possible that the diffusion rate of Fe and Mg was more sluggish in diopside in comparison to low-Ca pyroxene and olivine. McSween and Patchen (1989) also found

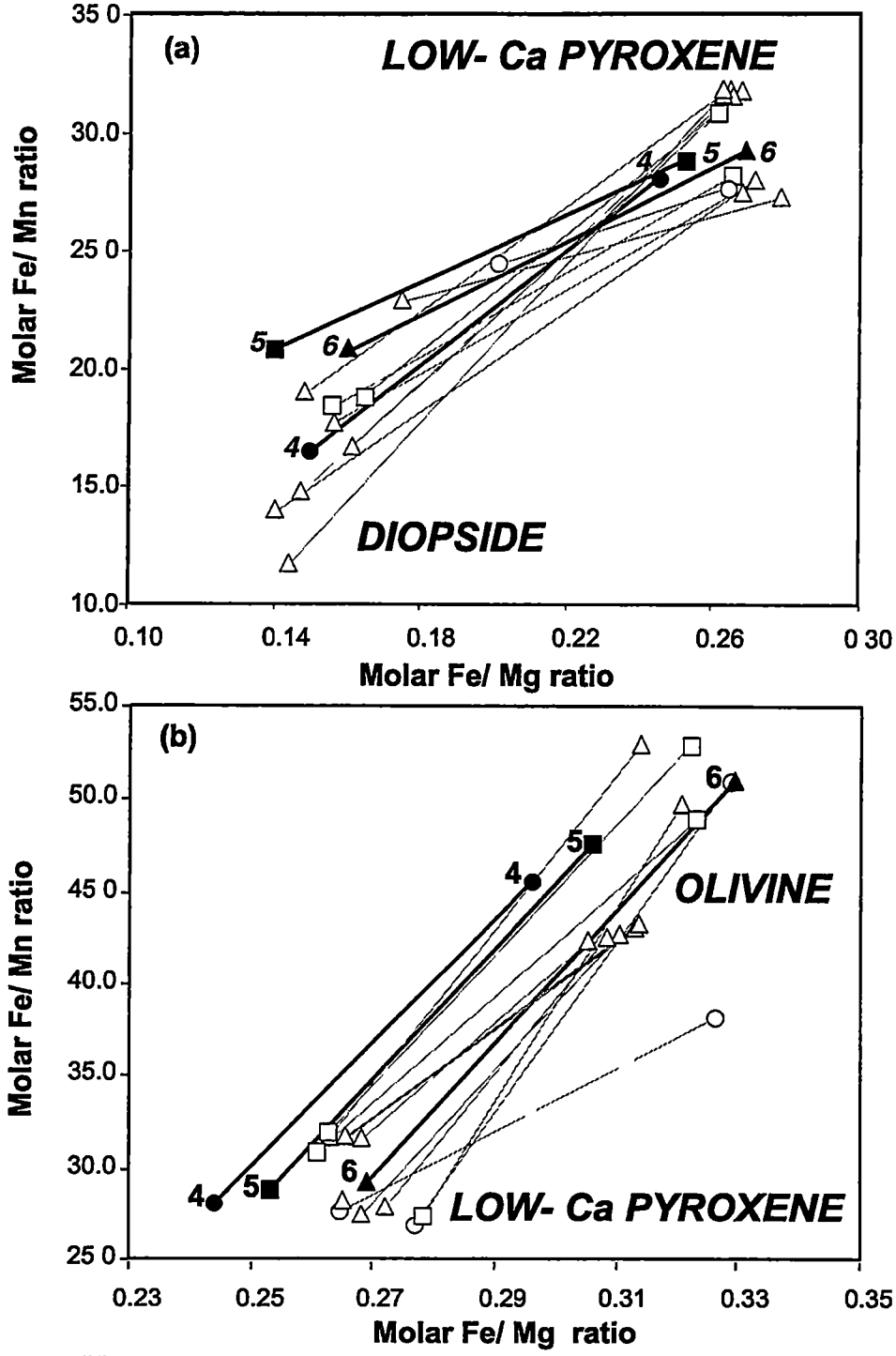

Figure 9: Tie lines connect diopside and low-Ca pyroxene (a) and olivine and low-Ca pyroxene (b) of same petrologic type in L chondrites. The black tie lines representing data from this study do not intersect between olivine and low-Ca pyroxene, whereas diopside and low-Ca pyroxene tie lines do cross. For the most part, tie lines connecting data collected from the literature (referenced in Fig. 6) intersect one another in (a) and (b).

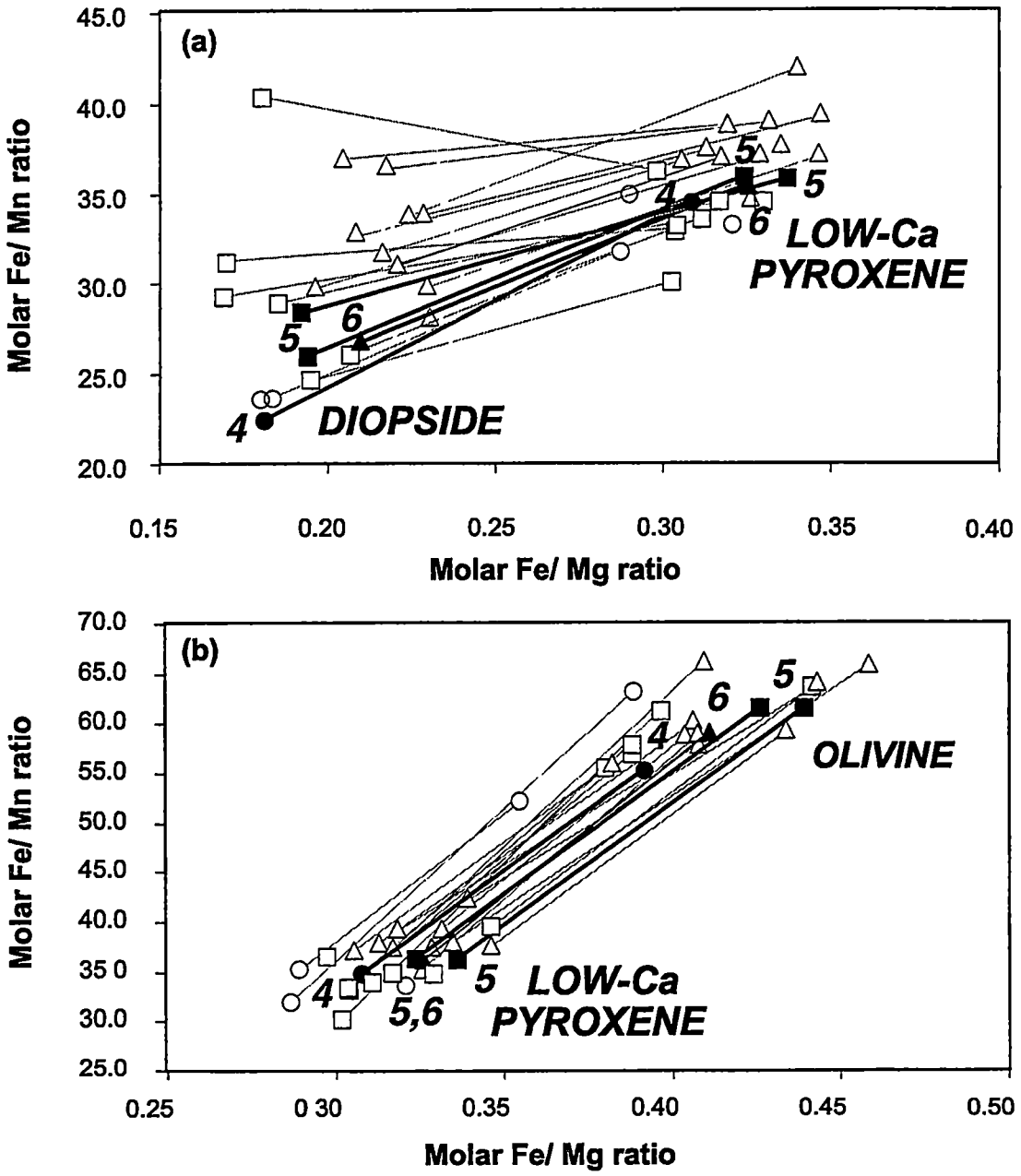

Figure 10: Tie lines connect olivine and low-Ca pyroxene (a) and diopside and low-Ca pyroxene in (b) of same petrologic type in LL chondrites. The black tie lines representing data from this study, intersect one another in both figures (a) and (b) as well as those tie lines connecting data collected from the literature (referenced in Fig. 7).

evidence for disequilibrium in the Ca contents of coexisting low-Ca pyroxene and diopside in LL6 chondrites. They speculated two possible reasons for disequilibrium: (1) gradational boundaries and (2) re-equilibrium during cooling. Upon cooling, silicate minerals of same petrologic type experienced identical peak metamorphic temperatures; however, during cooling differences in the degree of re-equilibration occurred. A steeper slope of the solvus limb for low-Ca pyroxene requires little compositional change with decreasing temperature as opposed to diopside, which requires a greater compositional change. Diffusion of Fe/Mg occurs at temperatures lower than Ca, so they may also re-equilibrate upon cooling. Thus, Fe and Mg in olivine continued to diffuse to a lower temperature compared to low-Ca pyroxene and diopside and, therefore, the olivine and low-Ca pyroxene and diopside and low-Ca pyroxene did not reach equilibrium in terms of Fe/Mn and Fe/Mg during cooling. McSween and Patchen (1989) also suggest that disequilibrium may stem from inherited Ca contents of low-Ca pyroxene in polymorphic forms prior to metamorphic recrystallization.

Minor Oxides

Finally, the abundance of minor oxides, CaO and TiO_2, in pyroxenes were affected during metamorphism. The L and LL chondrites demonstrate an increase in the CaO content of low-Ca pyroxene and a CaO decrease within diopside. I suggest that during metamorphism calcium was mobilized and removed from diopside and transferred to low-Ca pyroxene. The TiO_2 increase in low-Ca pyroxene with petrologic type of L and LL chondrites is identical to the results of Kamatsu and Miyamoto (1999). They proposed that the TiO_2 content

increased during metamorphism because it is easily taken into the low-Ca pyroxene.

Application to Reflectance Spectroscopy and the NEAR mission

The reflectance spectra of an asteroid's surface vary with its mineral abundances and compositions. Three important spectral features in the visible-near infrared (VIS-NIR) region are used to identify mineral abundances and composition on an asteroid surface (Fig. 11): (1) the area ratio of the 2 μm and 1 μm absorption bands (Band II/ Band I), which is a function of the olivine/ pyroxene abundance ratio (Cloutis et al., 1986), (2) the 1 μm band position (Band I center) controlled mostly by the Ca^{2+} content of pyroxene (Adams, 1974), and (3) the 2 μm band position (Band II center) giving the pyroxene Fe^{2+} content (Adams, 1974).

Figure 12a illustrates the spectra features of seven different S asteroid types (Gaffey et al., 1993), each representing a portion of a continuous suite of silicate phases ranging from pure olivine (Band II/ Band I = 0.0) to pure pyroxene (2.8 > Band II/ Band I > 1.6). The silicate surface mineralogy of S(IV) asteroids is composed of both olivine and low-Ca orthopyroxene. Ordinary chondrites were suggested to have mineral assemblages similar to S(IV) objects (Gaffey et al., 1993). To support this relationship, Murchie and Pieters (1996) found that laboratory spectra of specific H, L, and LL chondrites plot within the S(IV) asteroid field. Gaffey and Gilbert (1998) compiled laboratory spectra, also

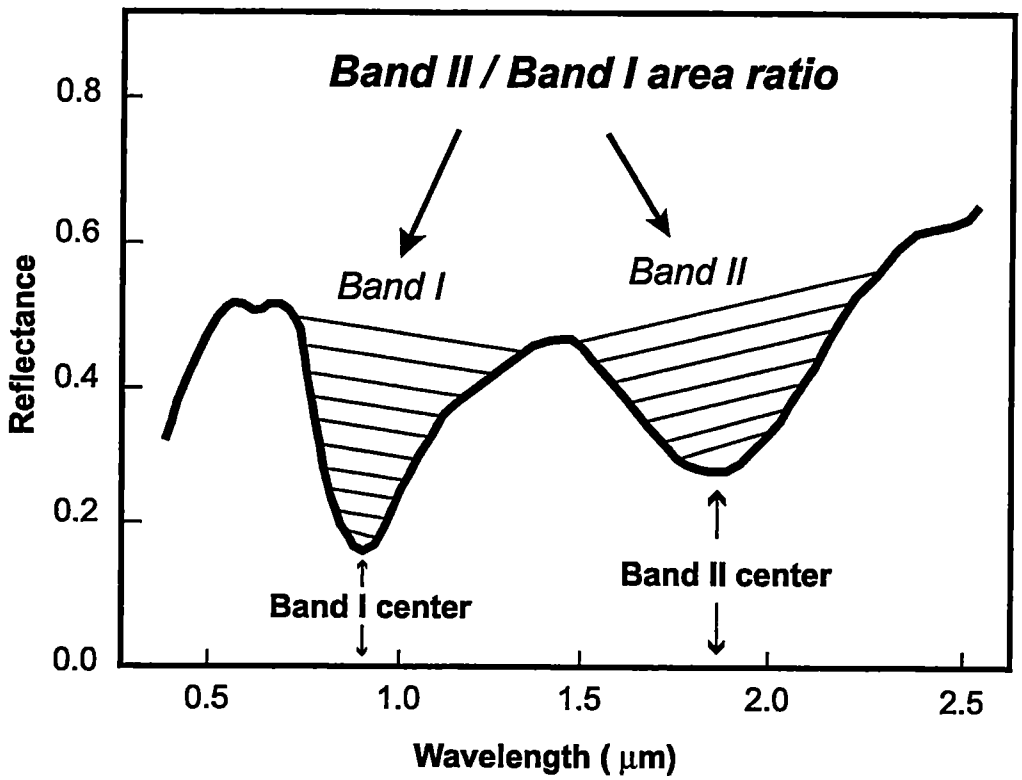

Figure 11: A schematic reflectance spectrum of an S-type asteroid, after McSween (1991), shows spectral parameters which are sensitive to silicate mineralogy found in meteorites. The characteristic spectra are used to identify mineral abundances and compositions on the surface of an asteroid or of a meteorite powder in the laboratory. The Band II/ Band I area ratio is a function of the olivine and pyroxene abundance (Cloutis et al., 1986), the Band I center reflects the Ca^{2+} pyroxene content (Adams, 1974), and the Band II center represents the Fe^{2+}content in pyroxene (Adams, 1974).

plotting in the S(IV) asteroid field, of different petrologic types of the L and LL chondrites (Fig. 12b). These numerous findings suggest that S(IV) asteroids have a strong affinity to the ordinary chondrite group. Interestingly, the spectra of LL5 chondrites suggest higher average olivine and pyroxene abundances compared to the LL6 chondrites; however, only spectra of two LL5 chondrites were obtained for the study.

Variations observed in rotational spectra indicate local variations in surface mineralogy for S asteroids 8 Flora, 15 Eunomia, and 6 Hebe (Gaffey, 1984; Gaffey and Ostro, 1987; Gaffey and Gilbert, 1998). McSween (1992) and Gaffey and Gilbert (1998) hypothesized that these spectral variations were attributed to rubble-pile structures, which allow different metamorphic grades of ordinary chondrites to be exposed on an asteroid surface. However, the spectral variations associated with oxidation during metamorphism may account for the variation of S-asteroid rotational spectra.

Perhaps the first spacecraft mission to orbit an S-type asteroid, 433 Eros, will enlighten the spectral interpretation of these bodies. One goal of the Near Earth Asteroid Rendezvous Shoemaker (NEAR) mission to Eros is to characterize and map the surface mineralogy of the asteroid using VIS-NIR spectra. A Near-Infrared Spectrometer (NIS) instrument aboard the spacecraft was developed to measure the spectrum of sunlight reflected from the surface of Eros in the 0.8-2.6 μm wavelength range with a resolution of 0.02-0.04 μm (Peacock et al., 1998). The spectra collected from Eros will be processed and cataloged according to a

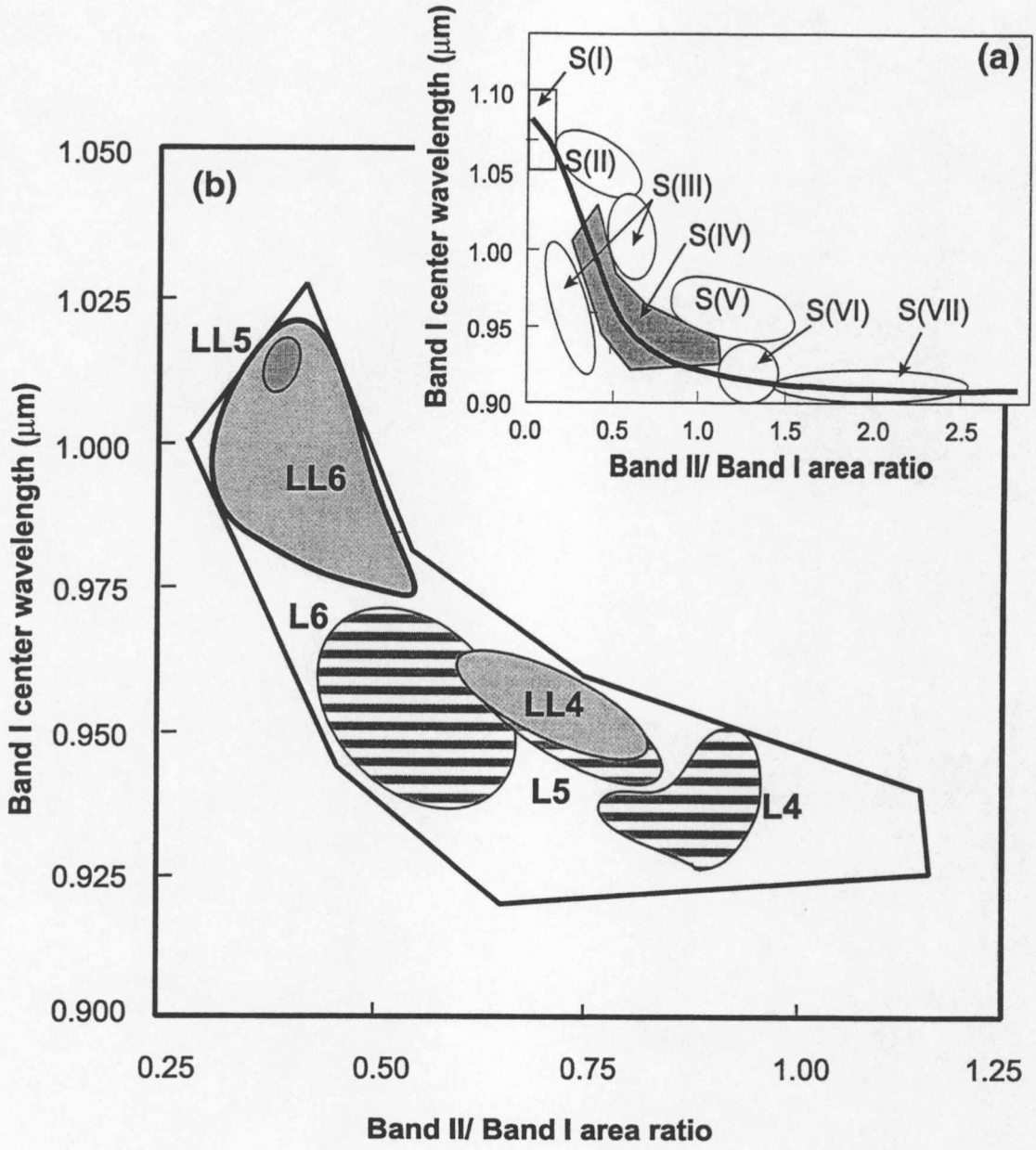

Figure 12: (a) Seven different types of S asteroids have been identified ranging from a continuous suite of silicate phases, pure olivine (Band II/ Band I=0.0) to pure pyroxene (2.8 > Band II/ Band I > 1.6) (Gaffey et al., 1993). The solid curve represents a simple olivine-orthopyroxene mixing line (Cloutis et al., 1986). The S(IV) type asteroids have a surface silicate mineralogy similar to the ordinary chondrites (Gaffey et al., 1993). (b) The laboratory spectra of petrologic types 4, 5, and 6 of L and LL chondrites plot within the S(IV) asteroid field (Gaffey and Gilbert, 1998).

mineral library so that the mineralogy of the asteroids surface is acquired. From the compiled information, the following questions may be addressed: (1) Does Eros have a rubble-pile structure?, and (2) Are the mineralogy and composition of Eros consistent with a chondritic surface assemblage?

Previous spectra have been collected and compiled from Earth-based observations of Eros, revealing a composite VIS-NIR spectrum. The average spectrum of Eros plots within the S(IV) asteroid group and exhibits mafic mineral absorptions consistent with the olivine-pyroxene assemblages in ordinary chondrites (Fig. 13). Rotational spectra of Eros reveal two different faces, one having a short-wavelength Band I, and the second located at a longer wavelength, with a broad, weaker Band I. The cause of the two distinct spectra may be attributed to uncertainty in the data, particle size differences, differences in "space weathering" effects, or compositional differences (Murchie and Pieters, 1996). The most plausible reason for the different spectra are compositional differences and suggest an olivine-rich face (estimated at $22^{\pm}7\%$ pyroxene and $78^{\pm}7\%$ olivine) and a pyroxene-rich face (estimated at $39^{\pm}10\%$ pyroxene and $61^{\pm}10\%$ olivine) (Murchie and Pieters, 1996).

Spectral data of 433 Eros suggests that it may have a rubble-pile structure composed of various petrologic types. This study focuses on L and LL ordinary chondrites and has applications for the continued study and research of mapping Eros.

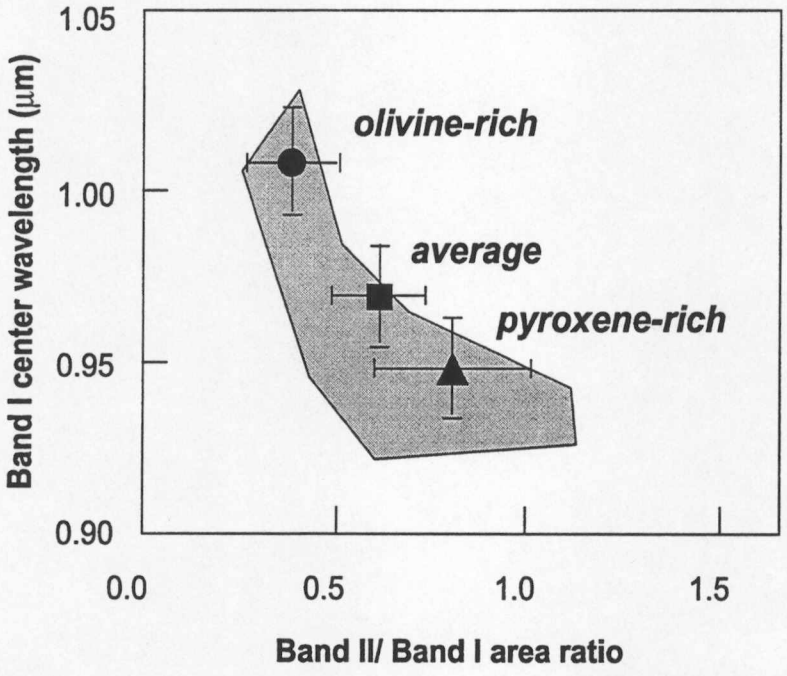

Figure 13: VIS-NIR spectra of 433 Eros, after Murchie and Pieters (1996), reveal an average spectrum, and two different compositional faces of Eros: olivine-rich and pyroxene-rich. The spectral data plots within the S(IV) asteroid field.

5. CONCLUSIONS

In this thesis I have presented the modal mineralogy and electron microprobe analyses for olivine, low-Ca pyroxene, and diopside for selected L and LL ordinary chondrites. The conclusions drawn from this data are consistent with the hypothesis that the oxidation reaction:

$$Fe + \frac{1}{2} O_2 + (Mg, Fe)SiO_3 \Rightarrow (Mg, Fe)_2SiO_4$$

metal pyroxene olivine

(McSween and Labotka, 1993) takes place during metamorphism.

1. The modal olivine: low-Ca pyroxene ratio mimics the trend observed in normative mineralogy (McSween et al., 1991) and increases with petrologic type. From the oxidation reaction, this ratio indicates that oxidation causes the olivine abundance to increase at the expense of low-Ca pyroxene and metal with progressive metamorphism.

2. Modal mineralogy also reveals a silica phase present in petrologic types 4, 5, and 6. The modal abundance of plagioclase increases with petrologic type and suggests that glass is still present in types 5 and 6. This is inconsistent with the absence of glass that Van Schmus and Wood (1967) used as one criterion to identify petrologic types 5 and 6.

3. A discrepancy exists between the modal and normative olivine: low-Ca pyroxene ratios. I suggest that the inconsistency is attributed to one or more of the following: sample bias in either the bulk chemical analysis and/ or the thin-section, and also the fact that these chondrites are extremely reduced, metal-bearing rocks suggests that the norm calculation procedure might not be appropriate.

4. The molar Fe/Mn and Fe/Mg of olivine and low-Ca pyroxene increase with petrologic types 4 to 6, whereas diopside does not exhibit this trend in the L chondrites. For the LL chondrites, the molar Fe/Mn and Fe/Mg of olivine and low-Ca pyroxene in type 5 is higher than type 6; however, Fe/Mn and Fe/Mg in diopside increase with petrologic types 4 to 6. As metal is oxidized with progressive metamorphism of ordinary chondrites, the Fe^{2+} diffuses and enriches the silicate minerals.

5. Examination of tie lines that connect olivine and low-Ca pyroxene and diopside and low-Ca pyroxene reveal all tie lines are roughly parallel and approach equilibrium in terms of Fe/Mn and Fe/Mg; however, the intersection of many tie lines implies disequilibrium in respect to these molar ratios. Possible explanations for disequilibrium are (1) boundaries between petrologic types are arbitrary breaks in a gradational sequence, and (2) cooling upon peak metamorphism allows Fe and Mg to continue to diffuse to a lower temperature in olivine compared to low-Ca pyroxene and diopside.

6. Characteristic spectral absorption features in the VIS-NIR region are sensitive to the olivine/ pyroxene abundance ratio (Cloutis et al., 1986) and the Ca^{2+} and Fe^{2+} contents of pyroxenes (Adams, 1974). Therefore, these spectral features can be used to identify the olivine/ pyroxene abundance ratios and pyroxene compositions on the surface of an asteroid. The H, L, and LL chondrites have distinct olivine/ pyroxene abundances and pyroxene compositions and are able to be correctly identified. This work shows that the different petrologic types of L and LL chondrites also have different olivine: low-Ca pyroxene abundances and pyroxene compositions and therefore, they should be able to be identified using VIS-NIR spectra. Furthermore, the mineralogy determined from spectral signatures is calculated using normative mineralogy and since the modal and normative olivine: low-Ca pyroxene ratios are offset, a calibration factor can be applied to establish the true olivine: low-Ca pyroxene ratio. Thus, the specific petrologic type can be identified.

REFERENCES

REFERENCES

ADAMS J. (1974) Visible and near-infrared diffuse reflectance spectra of pyroxenes as applied to remote sensing of solid objects in the solar system. *J. Geophys. Res.* **79,** 4829-4836.

ANDERS E. (1978) Most stony meteorites come from the asteroid belt. In *Asteroids: An Exploration Assessment* (eds. D. Morrison and W. C. Wells), pp. 57-75. NASA CP 2053.

BARYSHNIKOVA G. V., STAKHEYEVA S. A. IGNATENKO K. I. AND LAVRUKHINA A. K. (1985) Pyroxenes in H- and L-group ordinary chondrites. *Geochem. Intern.* **22,** 78-91.

BENNETT M. E. III AND MCSWEEN H. Y. Jr. (1996) Revised model calculations for the thermal histories of ordinary chondrite parent bodies. *Meteoritics* **31,** 783-792.

BERKLEY J. L., KEIL K., GOMES C. B. AND CURVELLO W. S. (1978) Studies of Brazilian meteorites XII. Mineralogy and petrology of the Santa Bárbara, Rio Grande do Sul, chondrite. *An. Acad. Brasil Ciênc.* **50,** 191-196.

BRETT R. AND SATO M. (1984) Intrinsic oxygen fugacity measurements on seven chondrites, a pallasite, and a tektite and the redox state of meteorite parent bodies. *Geochim. Cosmochim. Acta* **48,** 111-120.

CLOUTIS E. A., GAFFEY M. J., JACKOWSKI T. L. AND REED K. L. (1986) Calibrations of phase abundance, composition,and particle size distribution for olivine-orthopyroxene mixtures from reflectance spectra. *J. Geophys. Res.* **91,** 11,641-11,653.

GAINES R. V., SKINNER H. C. W., FOORD E. E., MASON B. AND ROSENZWEIG A. (eds.) (1997) *Dana's New Mineralogy- The System of Mineralogy of James Dwight Dana and Edward Salisbury Dana.* 8th ed. John Wiley and Sons, New York, New York, USA. 1819 pp.

DAVIS D. R., CHAPMAN C. R., WEIDENSCHILLING S. J. AND GREENBERG R. (1985) Collisional history of asteroids: Evidence from Vesta and the Hirayama families. *Icarus* **62,** 30-53.

DEER W. A., HOWIE R. A. AND ZUSSMAN J. (1997) *An Introduction to the Rock-Forming Minerals.* 2nd ed. Longman Group Ltd., London, UK. 696 pp.

DODD R. T. (1969) Metamorphism of ordinary chondrites: A review. *Geochim. Cosmochim. Acta* **33,** 1161-1203.

DODD R. T. (1974) Petrology of the St. Mesmin chondrite. *Contrib. Mineral. Petrol.* **31,** 201-227.

DODD R. T. (1976) Iron-silicate fractionation within ordinary chondrite groups. *Earth Planet. Sci. Lett.* **28,** 479-484.

DODD R. T. (1981) *Meteorites: A Petrologic-Chemical Synthesis.* Cambridge Univ. Press, New York, New York, USA. 368 pp.

DODD R. T. AND JAROSEWICH E. (1981) Chemical variations among L-group chondrites, III. Major element variation in L6 chondrites. *Meteoritics* **16,** 93-111.

FREDRIKSSON K., NELEN J. AND FREDRIKSSON B. J. (1968) The LL-group chondrites. In *Origin and Distribution of the Elements* (ed. L. H. AHRENS), pp. 457-466. Pergamon Press, New York, New York, USA.

GAFFEY M. J. (1984) Rotational spectral variations of asteroid (8) Flora: Implications for the nature of the S-type asteroids and for the parent bodies of the ordinary chondrites. *Icarus* **60,** 83-144.

GAFFEY M. J. (1999) Improving methodologies for quantitative interpretation of S(IV) / OC type: Asteroidal spectra with applications for the NEAR Eros Mission (abstract). *Proc. Lunar Planet. Sci. Conf.* **30,** #1375, Lunar and Planetary Institute, Houston, Texas, USA (CD-ROM).

GAFFEY M. J. AND GILBERT S. L. (1998) Asteroid 6 Hebe: The probable parent body of the H-type ordinary chondrites and the IIE iron meteorites. *Meteoritics* **33,** 1281-1295.

GAFFEY M. J. AND OSTRO S. J. (1987) Surface lithologic heterogeneity and body shape for asteroid 15 Eunomia (abstract). *Proc. Lunar Planet. Sci. Conf.* **18,** 310-311.

GAFFEY M. J., BELL J. F., BROWN R. H., BURBINE T. H., PLATEK J. L., REED K. L. AND CHAKY D. A. (1993) Mineralogical variations within the S-type asteroid class. *Icarus* **106,** 573-602.

GOODRICH C. A. AND DELANEY J. S. (2000) Fe/Mg-Fe/Mn relations of meteorites and primary heterogeneity of primitive achondrite parent bodies. *Geochim. Cosmochim. Acta* **64,** 149-160.

HARVEY R. P., BENNETT M. E. AND MCSWEEN H. Y. (1993) Pyroxene equilibration temperatures in metamorphosed ordinary chondrites (abstract). *Lunar Planet. Sci. Conf.* **24,** 615-616.

HEYSE J. V. (1978) The metamorphic history of LL-group ordinary chondrites. *Earth Planet. Sci. Lett.* **40,** 365-381.

HELGESON H. C., DELANY J. M., NESBITT H. W. AND BIRD D. K. (1978) Summary and critique of the thermodynamic properties of the rock forming minerals. *Amer. J. Sci.* **278-A,** 1-229.

HOLLAND T. J. B. AND POWELL R. (1990) An enlarged and updated internally consistent thermodynamic dataset with uncertainties and correlations: The system K_2O-Na_2O-CaO-MgO-MnO-FeO-Fe_2O_3-Al_2O_3-TiO_2-SiO_2-C-H_2-O_2. *J. Metam. Geol.* **8,** 89-124.

JAROSEWICH E. (1990) Chemical analyses of meteorites: A compilation of stony and iron meteorite analyses. *Meteoritics* **25,** 323-337.

KEIL K. AND FREDRIKSSON K. (1964) The Fe, Mg and Ca distribution in coexisting olivines and rhombic pyroxenes of chondrites. *J. Geophys. Res.* **69,** 3487-3515.

KEIL K., LANGE D., ULBRICH M. N. C., GOMES C. B., JAROSEWICH E., ROISENBERG A. AND SOUZA M. J. (1978) Studies of Brazilian meteorites XIII. Mineralogy, petrology, and chemistry of the Putinga, Rio Grande Do Sul, chondrite. *Meteoritics* **13,** 165-175.

KOMATSU M. AND MIYAMOTO M. (1999) Behavior of minor elements in olivine and orthopyroxene during metamorphism in LL chondrites (abstract). *Antarctic Meteorites XXIV,* 85-87.

LANGE D. E., MOORE C. B. AND RHOTON K. (1973) The Willowbar meteorite. *Meteoritics* **8,** 201-256.

MADARIS G. (1969) Partitioning of Fe^{++} and Mg^{++} between coexisting synthetic olivine and orthopyroxene. *Amer. J. Sci.* **267,** 945-968.

MASON B. (1979) In *Cosmochemistry Part 1. Meteorites in Data of Geochemistry.* 6th ed. (ed. M. FLEISCHER) U.S.G.S. Prof. Paper 440-B-1.

MCSWEEN H. Y. (1992) Redox effects in ordinary chondrites and implications for asteroid spectrophotometry. *Icarus* **95,** 239-243.

MCSWEEN H. Y. AND LABOTKA T. C. (1993) Oxidation during metamorphism of the ordinary chondrites. *Geochim. Cosmochim. Acta* **57,** 1105-1114.

MCSWEEN H. Y. AND PATCHEN A. D. (1989) Pyroxene thermobarometry in LL-group chondrites and implications for parent body metamorphism. *Meteoritics* **24,** 219-226.

MCSWEEN H. Y., BENNETT M. E. III AND JAROSEWICH E. (1991) The mineralogy of ordinary chondrites and implications for asteroid spectrophotometry. *Icarus* **90,** 107-116.

MINSTER J. F. AND ALLEGRE C. J. (1979) ^{87}Rb-^{87}Sr chronology of H chondrites: Constraint and speculations on the early evolution of their parent body. *Earth Planet. Sci. Lett.* **42,** 333-347.

MORGAN J. W., JANSSENS M.J., TAKAHASHI H., HERTOGEN J. AND ANDERS E. (1985) H-chondrites: Trace element clues to their origin. *Geochim. Cosmochim. Acta* **49,** 247-259.

MIYAMOTO M., FUJII N. AND TAKEDA, H. (1981) Ordinary chondrite parent body: An internal heating model (abstract). *Proc. Lunar Planet. Sci. Conf.* **12th,** 1145-1152.

MURCHIE S. L. AND PIETERS C. M. (1996) Spectral properties and rotational spectral heterogeneity of 433 Eros. *J. Geophys. Res.* **101,** 2201-2214.

PEACOCK K., WARREN J. W. AND DARLINGTON E. H. (1998) The Near infrared spectrometer. *Johns Hopkins APL Technical Digest* **19,** 115-124.

PELLAS R. AND STORZER D. (1981) ^{244}Pu fission track thermometry and its application to stony meteorites. *Proc. R. Soc. London* **374,** 253-270.

RUBIN A. E. (1990) Kamacite and olivine in ordinary chondrites: Intergroup and intragroup relationships. *Geochim. Cosmochim. Acta* **54,** 1217-1232.

RUBIN A. E. (1993) Metallic copper in ordinary chondrites. *Meteoritics* **29,** 94-98.

SEARS D. W. G. AND WEEKS K. S. (1986) Chemical and physical studies of type 3 chondrites: VI: Siderophile elements in ordinary chondrites. *Geochim. Cosmochim. Acta* **50,** 2815-2832.

SCORZELLI R. B., MICHEL-LÉVY M. C., GILABERT E., LAVIELLE B., AZEVEDO I. S., VIEIRA V. W., COSTA T. V. V. AND ARAÚJO M. A. B. (1998) The Campos Sales meteorite from Brazil: A lightly shocked L5 chondrite fall. *Meteoritics* **33,** 1335-1337.

SCOTT E. R. D. AND RAJAN R. S. (1981) Metallic minerals, thermal histories, and parent bodies of some xenolithic, ordinary chondrites. *Geochim. Cosmochim. Acta* **45,** 53-67.

SHERVAIS J. W., TAYLOR L. A., CIRLIN E., JAROSEWICH E. AND LAUL J. C. (1986) The Maryville Meteorite: A 1983 Fall of an L6 chondrite. *Meteoritics* **21,** 33-45.

SIGHINOLFI G. P., GARUTI G. AND MORAIS E. (1991) The Jolomba, Angola LL6 chondrite. *Meteoritics* **26,** 27-29.

SMITH D. G. W., BELL J. D. AND FRISCH T. (1972) The Timersoi, Niger, hypersthene chondrite. *Meteoritics* **7,** 1-16.

STÖFFLER D., KEIL K. AND SCOTT E. R. D. (1991) Shock metamorphism of ordinary chondrites. *Geochim. Cosmochim. Acta* **55,** 3845-3867.

TAYLOR L. A., PATCHEN A., TAYLOR D. S. AND CHAMBERS J. G. (1996) X-Ray digital imaging petrography of lunar mare soils: Modal analyses of minerals and glasses. *Icarus* **124,** 500-512.

UREY H. C. AND CRAIG H. (1953) The composition of the stone meteorites and the origin of the meteorites. *Geochim. Cosmochim. Acta* **4,** 36-82.

VAN SCHMUS W. R. AND WOOD J. A. (1967) A chemical-petrologic classification for the chondritic meteorites. *Geochim. Cosmochim. Acta* **31,** 747-765.

WILLIAMS C. V., RUBIN A. E., KEIL K. AND MIGUEL A. S. (1985) Petrology of the Cangas De Onis and Nulles regolith breccias: Implications for parent body history. *Meteoritics* **20,** 331-345.

WILLIAMS R. J. (1971a) Equilibrium temperatures, pressures, and oxygen fugacities of the equilibrated chondrites. *Geochim. Cosmochim. Acta* **35,** 407-411.

WILLIAMS R. J. (1971b) Reaction constants in the system Fe-MgO-SiO_2-O_2 at 1 atm, between 900 and 1300°C: Experimental results. *Amer. J. Sci.* **270,** 334-360.

WOOD J. A. (1967) Chondrites: Their metallic minerals, thermal histories, and parent bodies. *Icarus* **6,** 1-49.

APPENDICES

Appendix A: Modal Abundances

TABLE A-1. Total number of EDS spectra acquired for each phase.

Phases Present	Greenwell Springs	Homestead	Girgenti	Bald Mountain	Olivenza (1)	Olivenza (2)	Tuxtuac	Saint-Severin
Olivine	38009	64553	192040	110977	172876	363458	167470	186276
Orthopyroxene	21009	50313	122673	90292	68845	162345	68895	77134
Plagioclase	9290	15686	58074	24537	46323	107735	42945	50319
Diopside	2523	4628	25038	6747	14459	26391	17467	20963
Pigeonite	4476	7258	7778	22476	10347	13301	9178	5873
Troilite	4921	8636	27524	18928	12928	30142	19278	15962
Taenite	580	1123	4001	2206	2484	10329	3880	1932
Kamacite	283	8881	8068	10970	161	822	171	888
Chromite	565	928	3151	1521	2786	4177	2453	2622
Ilmenite	4	0	21	8	13	57	113	0
Whitlockite	734	838	2981	2210	2904	3895	1653	1384
K-rich glass	358	112	NA	287	816	1347	978	NA
Silica phase	7762	13093	NA	24504	21370	29388	17973	NA
Unclassified	8137	11947	59418	27492	28204	46009	34807	41243
Total	98651	187996	510767	343155	384516	799396	387261	404596

TABLE A2. Conversion of modal abundances (area %) to weight %.

Column	Procedure
1	Modal mineralogy produced by *Feature Scan* given in area %.
2	Subtract the unclassified and normalize to 100%. Equation to normalize: (Area % (from column 1))* (100/ (100-unclassified)).
3	The density (Gaines et al., 1997) is needed for each phase present. The density of olivine and low-Ca pyroxene were determined by the mineral composition of the phase (Deer et al., 1996).
4	Column 2 (amount of phase present) is multiplied by column 3 (density of phase).
5	Normalize this column by total sum of column 5 to obtain column 6.
6	These are the true mineral abundances present in the section and are compared to normative mineralogy.
7	The normative mineralogy was determined by McSween et al. (1991).

TABLE A-3. Modal abundances of Bald Mountain (L4).

Column	1	2	3	4	5	6	7
Bald Mountain (L4)	Area %	Normalized Area %	Density of Phase	Normalized Area % * Density	Normalized Modal Mineralogy	Normative Mineralogy	Normative Phase
silica phase	7.14	7.76	2.66	20.65	5.74	-----	
K-rich glass	0.08	0.09	2.54	0.22	0.06	0.71	orthoclase
whitlockite	0.64	0.70	3.10	2.16	0 60	0.48	apatite
ilmenite	0.00	0.00	4.78	0.00	0.00	0.25	ilmenite
chromite	0.44	0.48	5.06	2.42	0.67	0.86	chromite
kamacite	3.20	3.48	7.90	27.48	7.64	9 84	metal (ka + ta)
taenite	0.64	0.70	8.14	5 66	1 58		
troilite	5.52	6.00	4.84	29.05	8.08	8.14	troilite
pigeonite	6.55	7.12	3.44	24.50	6.81	-----	
diopside	1.97	2.14	3.28	7.02	1.95	4.68	diopside
plagioclase	7.15	7.77	2 62	20.37	5.66	9.06	anorthite + albite
orthopyroxene	26.31	28.60	3 39	96.97	26.97	26.48	hypersthene (opx+pig)
olivine	32.34	35.16	3.50	123.06	34.23	39.50	olivine
unclassified	8.01						
Total	99.99	100.00		359.55	100.00	100.00	
Total-unclassified	91.98						

mode olivine/low-Ca pyroxene ratio: 1.01
norm olivine/low-Ca pyroxene ratio: 1.49

TABLE A-4. Modal abundances of Homestead (L5).

Column	1	2	3	4	5	6	7
Homestead (L5)	Area %	Normalized Area %	Density of Phase	Normalized Area % * Density	Normalized Modal Mineralogy	Normative Mineralogy	Normative Phase
silica phase	6.98	7.46	2 66	19.83	5 47	-----	
K-rich glass	0.06	0.06	2.54	0.16	0.04	0.77	orthoclase
whitlockite	0.45	0.48	3.10	1.49	0.41	0.64	apatite
ilmenite	0	0.00	4.78	0.00	0.00	0.25	ilmenite
chromite	0 49	0 52	5.06	2 65	0 73	0.82	chromite
kamacite	4.73	5.05	7.90	39.91	11.01	9.44	metal (ka + ta)
taenite	0.6	0.64	8 14	5.22	1.44		
troilite	4.6	4.91	4.84	23.78	6.56	5 85	troilite
pigeonite	3.87	4.13	3.44	14.22	3.92	-----	
diopside	2 27	2.42	3.28	7.95	2.19	4.44	diopside
plagioclase	8.36	8.93	2.62	23.40	6.45	9 6	anorthite + albite
orthopyroxene	26.81	28.64	3.39	97.08	26.78	25.57	hypersthene (opx+pig)
olivine	34.4	36.74	3.45	126.77	34.98	42.62	olivine
unclassified	6.37						
Total	99.99	100.00		362.45	100.00	100.00	
Total-unclassified	93.62						

mode olivine/low-Ca pyroxene ratio: 1.14
norm olivine/low-Ca pyroxene ratio: 1.67

TABLE A-5. Modal abundances of Girgenti (L6).

Column	1	2	3	4	5	6	7
Girgenti (L6)	Area %	Normalized Area %	Density of Phase	Normalized Area % * Density	Normalized Modal Mineralogy	Normative Mineralogy	Normative Phase
silica phase	NA	NA	2.66	N. A.	N. A	-----	
K-rich glass	NA	NA	2.54	N. A.	N. A.	0.59	orthoclase
whitlockite	0 58	0.66	3.10	2.04	0.58	0.57	apatite
ilmenite	0.00	0 00	4 78	0 00	0 00	0.23	ilmenite
chromite	0.62	0.70	5 06	3.55	1.00	0.72	chromite
kamacite	1.58	1.79	7.90	14.13	4.00	8 04	metal (ka + ta)
taenite	0 78	0.88	8.14	7.19	2.03		
troilite	5.39	6.10	4.84	29.52	8.36	6.47	troilite
pigeonite	1.52	1.72	3.44	5.92	1.68	-----	pigeonite
diopside	4.90	5.55	3.28	18.18	5.15	4.64	diopside
plagioclase	11.37	12.87	2.62	33 71	9.55	9.35	anorthite + albite
orthopyroxene	24.02	27.18	3.39	92.15	26.09	23.12	hypersthene (opx+pig)
olivine	37.60	42.55	3.45	146.81	41.57	46.27	olivine
unclassified	11.63						
Total	99.99	100.00		353.19	100.00	99.41	
Total-unclassified	88.36						

mode olivine/low-Ca pyroxene ratio: 1.50
norm olivine/low-Ca pyroxene ratio: 2.00

TABLE A-6. Modal abundances of Greenwell Springs (LL4).

Column	1	2	3	4	5	6	7
Greenwell Springs (LL4)	Area %	Normalized Area %	Density of Phase	Normalized Area % * Density	Normalized Modal Mineralogy	Normative Mineralogy	Normative Phase
silica phase	7.87	8 58	2 66	22.81	6.65	-----	
K-rich glass	0.36	0.39	2 54	1.00	0.29	0 65	orthoclase
whitlockite	0.74	0.81	3 10	2.50	0.73	0.5	apatite
ilmenite	0.00	0 00	4.78	0.00	0 00	0.21	ilmenite
chromite	0.57	0.62	5.06	3.14	0.91	0 79	chromite
kamacite	0 29	0.32	7.90	2 50	0.73	4.29	metal (ka + ta)
taenite	0.59	0.64	8.14	5.23	1.52		
troilite	4.99	5.44	4 84	26 32	7 67	4.76	troilite
pigeonite	4.54	4.95	3.44	17.02	4.96	-----	
diopside	2.56	2.79	3 28	9.15	2.66	5.65	diopside
plagioclase	9.42	10.27	2.62	26.90	7.83	9 51	anorthite + albite
orthopyroxene	21.30	23.21	3.40	78.92	22.99	21.61	hypersthene (opx+pig)
olivine	38.53	41.99	3 52	147.80	43 06	52.01	olivine
unclassified	8.25						
Total	100.01	100.00		343 29	100.00	99.98	
Total-unclassified	91.76						

mode olivine/low-Ca pyroxene ratio: 1.54
norm olivine/low-Ca pyroxene ratio: 2 41

TABLE A-7. Modal abundances of Olivenza (LL5) section 1.

Column	1	2	3	4	5	6	7
Olivenza (LL5) (section 1)	Area %	Normalized Area %	Density of Phase	Normalized Area % * Density	Normalized Modal Mineralogy	Normative Mineralogy	Normative Phase
silica phase	5.56	6.00	2.66	15 96	4.69	-----	
K-rich glass	0.21	0 23	2.54	0 58	0.17	0.59	orthoclase
whitlockite	0.76	0.82	3.10	2.54	0.75	0.60	apatite
ilmenite	0.00	0.00	4 78	0.00	0.00	0.23	ilmenite
chromite	0.72	0.78	5 06	3.93	1.15	0 85	chromite
kamacite	0.04	0.04	7.90	0 34	0.10	2 96	metal (ka + ta)
taenite	0.65	0.70	8.14	5 71	1 68		
troilite	3.36	3.63	4 84	17 55	5.16	5 09	troilite
pigeonite	2.69	2 90	3.44	9.99	2.93	-----	
diopside	3.76	4.06	3.28	13.30	3.91	4.88	diopside
plagioclase	12.05	13 00	2.62	34.07	10.01	9.85	anorthite + albite
orthopyroxene	17.90	19 32	3.40	65.68	19.29	21.68	hypersthene (opx+pig)
olivine	44 96	48.52	3.52	170.80	50.17	53 29	olivine
unclassified	7.33						
Total	99.99	100.00		340 45	100.00	100.02	
Total-unclassified	92.66						

mode olivine/low-Ca pyroxene ratio: 2.26
norm olivine/low-Ca pyroxene ratio: 2.46

TABLE A-8. Modal abundances of Olivenza (LL5) section 2.

Column	1	2	3	4	5	6	7
Olivenza (LL5) (section 2)	Area %	Normalized Area %	Density of Phase	Normalized Area % * Density	Normalized Modal Mineralogy	Normative Mineralogy	Normative Phase
silica phase	3.68	3 90	2.66	10 39	3 01	-----	
K-rich glass	0.17	0.18	2.54	0.46	0.13	0.59	orthoclase
whitlockite	0.49	0 52	3.10	1.61	0.47	0.60	apatite
ilmenite	0.01	0 01	4.78	0.05	0.01	0.23	ilmenite
chromite	0.52	0.55	5 06	2.79	0.81	0.85	chromite
kamacite	0.10	0 11	7.90	0 84	0 24	2.96	metal (ka + ta)
taenite	1.29	1 37	8 14	11.14	3.23		
troilite	3 77	4.00	4.84	19.36	5 62	5.09	troilite
pigeonite	1.66	1.76	3.44	6.06	1.76	-----	
diopside	3 30	3.50	3 28	11.48	3.33	4.88	diopside
plagioclase	13.48	14.30	2.62	37.47	10.87	9.85	anorthite + albite
orthopyroxene	20.31	21.55	3.40	73.27	21.25	21.68	hypersthene (opx+pig)
olivine	45.47	48.24	3.52	169.82	49.26	53 29	olivine
unclassified	5.76						
Total	100.01	100.00		344.73	100.00	100.02	
Total-unclassified	94.25						

mode olivine/low-Ca pyroxene ratio: 2.14
norm olivine/low-Ca pyroxene ratio: 2.46

TABLE A-9. Modal abundances of Tuxtuac (LL5).

Column	1	2	3	4	5	6	7
Tuxtuac (LL5)	Area %	Normalized Area %	Density of Phase	Normalized Area % * Density	Normalized Modal Mineralogy	Normative Mineralogy	Normative Phase
silica phase	4.64	5.10	2.66	13 56	3.92	-----	
K-rich glass	0.25	0.27	2.54	0.70	0.20	N. A.	orthoclase
whitlockite	0.43	0.47	3.10	1.47	0.42	N. A.	apatite
ilmenite	0.03	0.03	4.78	0.16	0.05	N. A.	ilmenite
chromite	0.63	0.69	5.06	3 50	1.01	N. A	chromite
kamacite	0.04	0.04	7.90	0.35	0.10	N. A.	metal (ka + ta)
taenite	1.00	1.10	8.14	8.95	2.59		
troilite	4.98	5.47	4.84	26.49	7.65	N. A.	troilite
pigeonite	2.37	2.60	3.44	8 96	2 59	-----	
diopside	4.51	4.96	3.28	16.25	4.70	N A.	diopside
plagioclase	11.09	12.19	2.62	31.93	9.23	N. A.	anorthite + albite
orthopyroxene	17.79	19.55	3.40	66.47	19.21	N. A.	hypersthene (opx+pig)
olivine	43 24	47 52	3.52	167.26	48.34	N A.	olivine
unclassified	8.99						
Total	99.99	100.00		346.02	100.00		
Total-unclassified	91.00						

mode olivine/low-Ca pyroxene ratio: 2 22

TABLE A-10. Modal abundances of Saint Severin (LL6).

Column	1	2	3	4	5	6	7
Saint Sevrin (LL6)	Area %	Normalized Area %	Density of Phase	Normalized Area % * Density	Normalized Modal Mineralogy	Normative Mineralogy	Normative Phase
silica phase	N. A.	N. A.	2.66	N. A.	N. A.	-----	
K-rich glass	N. A.	N. A.	2.54	N. A.	N. A.	0.65	orthoclase
whitlockite	0.34	0.38	3 10	1.17	0.34	0.52	apatite
ilmenite	0.00	0.00	4 78	0.00	0.00	0.21	ilmenite
chromite	0.65	0.72	5.06	3.66	1.06	0.86	chromite
kamacite	0.22	0.24	7.90	1.94	0.56	3.24	metal (ka + ta)
taenite	0.48	0.53	8.14	4.35	1.26		
troilite	3.95	4.40	4 84	21.29	6.16	5.81	troilite
pigeonite	1.45	1.61	3.44	5.55	1 61	-----	pigeonite
diopside	5.18	5.77	3.28	18.91	5.47	5 21	diopside
plagioclase	12.44	13 85	2.62	36.29	10.50	10.13	anorthite + albite
orthopyroxene	19.06	21.22	3.40	72.16	20.87	18.56	hypersthene (opx+pig)
olivine	46.04	51 26	3.52	180.45	52.19	54.82	olivine
unclassified	10.19						
Total	100.00	100 00		345.76	100.00	99.36	
Total-unclassified	89.81						

mode olivine/low-Ca pyroxene ratio: 2.32
norm olivine/low-Ca pyroxene ratio: 2.95

Appendix B: Electron Microprobe Data

TABLE B1. Electron microprobe data of olivine.

Olivine	BML4-1 [6]	BML4-2 [6]	BML4-3 [6]	BML4-4 [6]	HL5-1 [4]	HL5-2 [4]	HL5-3 [4]	HL5-4 [4]	GL6-1 [4]	GL6-2 [4]
SiO_2	38.0 (4)	38.1 (2)	38.5 (3)	38.1 (1)	37.9 (2)	38.1 (1)	37.8 (2)	37.6 (3)	38.4 (2)	38.3 (1)
TiO_2	< 0.03	< 0.03	< 0.03	< 0.03	< 0.03	< 0.03	< 0.03	0.08 (5)	n d.	< 0.03
Al_2O_3	< 0.03	< 0.03	< 0 03	< 0.03	< 0.03	< 0.03	< 0 03	< 0.03	< 0 03	< 0.03
Cr_2O_3	< 0.03	0.05 (9)	< 0 03	< 0.03	< 0 03	< 0.03	< 0 03	< 0.03	< 0.03	< 0.03
MgO	40.0 (3)	40.0 (1)	40 1 (1)	40.1 (2)	39.4 (1)	39.3 (0)	39.7 (1)	39.5 (2)	39.0 (5)	39.1 (2)
CaO	< 0.03	< 0.03	< 0.03	< 0.03	0.03 (1)	< 0.03	0.03 (2)	0.03 (2)	< 0 03	< 0.03
MnO	0.44 (4)	0.48 (4)	0.46 (3)	0.45 (2)	0.42 (4)	0.46 (4)	0.47 (4)	0 45 (4)	0.45 (2)	0.44 (2)
FeO	21.3 (3)	21.0 (1)	21 2 (2)	21 1 (4)	21 6 (1)	21.5 (3)	21.5 (2)	21.5 (2)	22.8 (4)	22.8 (2)
Na_2O	< 0.03	< 0.03	< 0.03	< 0.03	< 0.03	< 0.03	< 0.03	0.03 (2)	< 0.03	< 0.03
Total	99.84	99.76	100.36	99.95	99.36	99 43	99.65	99.18	100 68	100.73
cations based on 4 oxygen										
Si	0.988	0 990	0 994	0 988	0.990	0.994	0.987	0 986	0.994	0.992
Ti	0 000	0.000	0.000	0.000	0.000	0 000	0.000	0 002	0.000	0.000
Al	0.000	0.000	0.000	0.000	0.000	0.001	0.000	0.000	0.000	0 000
Cr	0.000	0.001	0.000	0.002	0.000	0.000	0 001	0.000	0.000	0 000
Mg	1.551	1.548	1.544	1.551	1.535	1.530	1 543	1.544	1.506	1.510
Ca	0.001	0.001	0.001	0.000	0.001	0.001	0.001	0.001	0.000	0.000
Mn	0.010	0.011	0.010	0.010	0.009	0.010	0.011	0.010	0.010	0.010
Fe	0.462	0.456	0.457	0.458	0.473	0.469	0.470	0.470	0.495	0 495
Na	0.000	0.001	0.000	0.001	0 000	0.001	0.000	0.000	0.000	0 000
Total	3.012	3.009	3.006	3.010	3.009	3.005	3.013	3.012	3.006	3.008
Fe/Mn	47.4	43.2	45.4	46.2	51.6	46.9	44.8	48.2	50 3	51.9
Fe/Mg	0.30	0 29	0.30	0.30	0.31	0.31	0.30	0.30	0.33	0.33

TABLE B1. Electron microprobe data of olivine.

GL6-3	GL6-4	GWLL4-1	GWLL4-2	GWLL4-3	GWLL4-4	OLL5-1-1	OLL5-2-1	OLL5-3-1	OLL5-4-1	OLL5-1-2
[4]	[4]	[6]	[6]	[6]	[6]	[4]	[4]	[4]	[4]	[4]
38 3 (2)	38.1 (1)	36.6 (3)	36 9 (3)	36.7 (2)	36 9 (5)	36.8 (2)	36 9 (1)	36 98	37 2 (1)	37.4 (2)
< 0.03	< 0.03	< 0.03	< 0.03	< 0.03	< 0.03	< 0.03	< 0.03	0.08 (2)	0.00	< 0.03
< 0.03	< 0 03	< 0 03	< 0.03	< 0.03	< 0 03	< 0 03	< 0.03	< 0.03	< 0 03	< 0.03
< 0.03	< 0.03	n.d.	< 0 03	0.03 (3)	< 0 03	< 0.03	< 0 03	0.03 (1)	< 0.03	< 0.03
38 8 (3)	38.6 (2)	36 5 (1)	36 5 (1)	36 4 (1)	36.7 (2)	35.1 (2)	35.1 (0)	35.0 (1)	35.2 (1)	35.4 (2)
< 0 03	< 0 03	< 0 03	0.03 (1)	< 0.03	0.03 (2)	0 04 (1)	0.05 (1)	0 05 (2)	0 04 (1)	0.03 (1)
0.44 (2)	0 45 (2)	0.49 (5)	0.46 (4)	0.45 (2)	0 44 (5)	0 44 (1)	0.41 (6)	0.44 (3)	0.44 (3)	0.47 (4)
22.9 (1)	22.9 (1)	25.5 (2)	25.7 (3)	25.6 (3)	25 5 (2)	26.6 (1)	26.7 (3)	26.7 (1)	26.6 (2)	26.7 (2)
< 0 03	n.d.	< 0 03	< 0.03	< 0.03	< 0.03	< 0.03	< 0.03	< 0 03	< 0.03	< 0.03
100.51	100.09	99.11	99 53	99.24	99 62	99.08	99.25	99.22	99.47	100.02
0 995	0 994	0.980	0.983	0 982	0.983	0.989	0.991	1 000	0.994	0.994
0.000	0.000	0.000	0.000	0 001	0.000	0.000	0.000	0.000	0.000	0.000
0.000	0.000	0.000	0.000	0.000	0.000	0.000	0.000	0.000	0.000	0 000
0.000	0.000	0.000	0.000	0.001	0.000	0 000	0.000	0.001	0.000	0.001
1.502	1.502	1.458	1 450	1 452	1.455	1.409	1.405	1.401	1.403	1.404
0.000	0.000	0 000	0.001	0.000	0.001	0.001	0.002	0 002	0.001	0.001
0.010	0.010	0.011	0.010	0.010	0.010	0.010	0.009	0 010	0 010	0.011
0.497	0.499	0.571	0.572	0.572	0 568	0.600	0.600	0.599	0 596	0.595
0.000	0.000	0.000	0.000	0.001	0.001	0.001	0.001	0.001	0 001	0.000
3.004	3.005	3.020	3.017	3.018	3 017	3.011	3.009	3.007	3.006	3 006
51 3	50.0	51.1	55.4	56.2	58.7	60.1	65.6	60 5	59.6	56.7
0.33	0.33	0.39	0.39	0.39	0 39	0.43	0.43	0 43	0.42	0.42

TABLE B1. Electron microprobe data of olivine.

OLL5-2-2 [4]	OLL5-3-2 [4]	OLL5-4-2 [4]	TLL5-1 [4]	TLL5-2 [4]	TLL5-3 [4]	TLL5-4 [4]	SSLL6-1 [4]	SSLL6-2 [4]	SSLL6-3 [4]	SSLL6-4 [4]
37.5 (3)	37.2 (1)	37.2 (2)	37.1 (1)	37.3 (2)	37.2 (2)	37.1 (1)	37.5 (3)	37.7 (1)	37.6 (2)	37.6 (1)
< 0.03	0.05 (0)	0.03 (1)	0.03 (4)	< 0.03	< 0.03	0.05 (3)	< 0.03	< 0.03	< 0.03	< 0.03
0.07 (8)	0.01 (1)	0.05 (3)	< 0 03	< 0.03	< 0.03	< 0.03	< 0.03	< 0 03	< 0.03	< 0.03
< 0.03	0 06 (3)	0.07 (5)	0.03 (3)	< 0 03	< 0.03	0.07 (7)	0.03 (2)	0.05 (1)	< 0.03	< 0.03
35.4 (4)	35 3 (2)	35.1 (1)	35.0 (1)	35.0 (1)	35.0 (4)	35.0 (1)	35.5 (2)	35.4 (1)	35.6 (4)	35.4 (2)
0.03 (1)	0.04 (2)	0.05 (1)	< 0.03	0.03 (2)	0.03 (2)	0 03 (1)	0.03 (2)	0 05 (1)	0.03 (2)	0.04 (3)
0.44 (1)	0.42 (1)	0.44 (2)	0 44 (2)	0.44 (1)	0.44 (2)	0.45 (2)	0.43 (5)	0.43 (3)	0.44 (4)	0.45 (3)
26 7 (2)	27.1 (1)	27 1 (1)	27.4 (3)	27 4 (3)	27 5 (2)	27.7 (2)	25.8 (7)	26.2 (2)	25.6 (8)	26.4 (2)
< 0.03	< 0.03	< 0 03	< 0 03	< 0 03	< 0.03	< 0 03	< 0.03	< 0 03	< 0 03	< 0 03
100.15	100.08	100.09	100.09	100.13	100.22	100.45	99.36	99.86	99.66	99.94
0.995	0.990	0.991	0 991	0.993	0.992	0.988	1.001	1 001	1.000	1.000
0.000	0.001	0.001	0.001	0 000	0.001	0.001	0.000	0 000	0.000	0.000
0 002	0.001	0.002	0.000	0.000	0.000	0.000	0.000	0.000	0.000	0.000
0 000	0.001	0 001	0 001	0.001	0.000	0.001	0 001	0 001	0.000	0.000
1.402	1.401	1.396	1.393	1.392	1 391	1.391	1.411	1.403	1.412	1.401
0.001	0.001	0.001	0.001	0.001	0.001	0.001	0.001	0.001	0.001	0.001
0.010	0.009	0.010	0.010	0.010	0.010	0.010	0.010	0.010	0.010	0.010
0.593	0.604	0.605	0.612	0.610	0.613	0.618	0.576	0.582	0.577	0.586
0.001	0.000	0.000	0.000	0.000	0.001	0.001	0.001	0.000	0.000	0.000
3.004	3.008	3.007	3.009	3.006	3.008	3.010	2.999	2 999	3.000	3.000
60.8	65 2	62.1	62.8	61.0	61 3	60.3	59.5	59.4	60.0	57.9
0.42	0.43	0.43	0.44	0.44	0.44	0.44	0.41	0.41	0.41	0 42

TABLE B2. Electron microprobe data of low-Ca pyroxene.

Low-Ca Pyroxene	BML4-1 [6]	BML4-2 [6]	BML4-3 [6]	BML4-4 [6]	BML4-5 [6]	BML4-6 [6]	BML4-7 [6]	BML4-8 [6]	HL5-1 [4]	HL5-2 [4]
SiO_2	55.8 (4)	55.6 (5)	56.1 (3)	55.8 (3)	56.1 (3)	56.0 (2)	56.1 (3)	55.9 (2)	55.3 (2)	54.7 (5)
TiO_2	0.14 (5)	0.20 (12)	0.10 (3)	0.17 (5)	0.08 (2)	0.07 (2)	0.08 (5)	0.12 (5)	0.16 (2)	0.16 (3)
Al_2O_3	0.13 (6)	0.26 (21	0 22 (12)	0.14 (5)	0.08 (2)	0.06 (1)	0.17 (11)	0.15 (7)	0.20 (4)	0.53 (10)
Cr_2O_3	0.09 (3)	0.19 (15)	0.16 (11)	0 07 (5)	0.08 (4)	0.07 (3)	0.16 (10)	0.12 (5)	0.15 (3)	0 40 (11)
MgO	30 4 (2)	29.7 (6)	29.8 (6)	30.1 (2)	30.0 (2)	29.9 (3)	29.8 (5)	30.0 (2)	29.6 (1)	28 9 (2)
CaO	0.28 (5)	0.51 (46)	0.61 (28)	0.43 (13)	0.23 (4)	0.30 (8)	0.67 (48)	0.43 (17)	0.52 (4)	1.07 (8)
MnO	0.45 (4)	0.48 (3)	0.48 (4)	0.46 (3)	0.44 (2)	0.45 (4)	0.46 (4)	0.46 (1)	0.49 (3)	0.43 (4)
FeO	13.1 (1)	13.0 (3)	12 8 (4)	13.2 (2)	13.1 (2)	13.2 (1)	12.9 (1)	13.0 (1)	13.2 (1)	13.2 (2)
Na_2O	< 0.03	< 0.03	0.05 (4)	< 0.03	< 0.03	< 0.03	< 0.03	< 0.03	< 0.03	< 0.03
Total	100.34	100.05	100.39	100.30	100.08	100.08	100.37	100.23	99.61	99.45
cations based on 6 oxygen										
Si	1.978	1.982	1.990	1.982	1.994	1.992	1.989	1.987	1.981	1.969
Ti	0.004	0.005	0.003	0.004	0.002	0.002	0.002	0.003	0.004	0 004
Al	0.005	0.011	0 009	0.006	0.003	0.002	0.007	0.006	0.008	0 022
Cr	0.005	0.005	0.004	0.002	0.002	0.002	0.004	0.004	0.004	0 011
Mg	1.608	1.579	1.577	1 594	1.588	1.587	1.578	1.587	1.580	1.551
Ca	0.011	0.020	0.023	0.016	0 009	0.012	0.026	0.016	0.020	0.042
Mn	0.014	0.014	0.015	0.014	0.013	0.014	0.014	0.014	0.015	0.013
Fe	0.388	0.388	0 379	0.391	0 390	0.393	0.383	0.387	0.395	0 396
Na	0.001	0.001	0.003	0.000	0.001	0.001	0.001	0.001	0 001	0.001
Total	4.013	4.005	4.002	4.009	4.001	4.004	4.003	4.005	4.008	4.011
Fe/Mn	28.4	27.1	26.1	28.3	29.6	29.1	28.2	28.1	26.6	29.9
Fe/Mg	0 24	0.25	0.24	0.25	0.25	0 25	0.24	0 24	0.25	0.26

TABLE B2. Electron microprobe data of low-Ca pyroxene.

HL5-3 [4]	HL5-4 [4]	GL6-1 [4]	GL6-2 [4]	GL6-3 [4]	GL6-4 [4]	GSLL4-1 [6]	GSLL4-2 [6]	GSLL4-3 [6]	GSLL4-4 [6]	GSLL4-5 [6]
55.1 (1)	55.7 (2)	55.0 (1)	55.0 (2)	55.6 (6)	55.5 (7)	54 9 (4)	55.1 (3)	55.1 (4)	54.6 (6)	55 0 (2)
0.08 (3)	0.11 (5)	0.18 (4)	0.20 (5)	0.15 (2)	0.21 (1)	0.12 (5)	0.08 (5)	0.11 (4)	0.16 (6)	0.12 (5)
0.08 (4)	0.10 (4)	0.14 (3)	0.18 (5)	0.14 (3)	0.16 (1)	0.12 (8)	0.12 (5)	0.15 (5)	0.35 (15)	0.12 (4)
0.15 (7)	0.08 (7)	0.11 (2)	0.13 (3)	0.12 (2)	0.11 (2)	0.09 (7)	0.11 (7)	0 10 (2)	0.42 (45)	0.09 (5)
29.6 (2)	29.8 (6)	28 9 (3)	29 1 (2)	29.3 (4)	28.8 (1)	28.1 (2)	27.8 (2)	27 7 (3)	27.6 (2)	28.1 (3)
0.51 (3)	0.50 (6)	0.79 (9)	0.78 (8)	0.78 (6)	0.87 (14)	0.56 (11)	0.40 (6)	0.66 (4)	0.68 (20)	0.32 (7)
0.43 (1)	0.48 (2)	0.47 (2)	0.44 (4)	0.49 (4)	0.48 (5)	0.44 (3)	0.47 (4)	0.42 (3)	0.48 (3)	0.44 (3)
13.4 (2)	13.5 (1)	13.9 (0)	13.9 (1)	13.8 (6)	14.0 (2)	15.2 (8)	15.6 (3)	15.4 (3)	15.7 (3)	15.5 (2)
< 0.03	< 0.03	< 0.03	< 0.03	< 0.03	< 0.03	< 0.03	< 0 03	< 0.03	< 0.03	< 0.03
99.34	100.27	99.52	99.77	100.43	100.24	99.59	99 66	99.62	100.03	99.72
1.981	1.982	1.979	1.975	1.982	1.985	1.985	1.993	1 991	1.973	1 987
0.002	0.003	0.005	0.006	0.004	0.006	0.003	0.002	0.003	0 004	0 003
0.003	0.004	0 006	0.008	0.006	0.007	0.005	0.005	0.006	0.015	0.005
0.030	0.002	0.003	0.004	0.003	0.003	0.003	0.003	0 003	0.012	0.002
1.586	1.583	1.554	1.560	1.558	1.536	1.516	1.498	1.494	1.489	1.514
0.020	0.019	0.031	0.030	0.030	0.034	0 022	0.015	0.026	0.027	0.013
0.013	0.014	0.015	0.013	0.015	0.015	0.014	0.015	0.013	0.015	0.014
0.404	0.402	0.419	0.419	0.412	0.419	0.461	0.471	0.466	0.476	0.467
0.001	0.001	0.001	0.001	0.001	0.001	0.001	0.001	0.002	0.001	0.001
4.014	4.012	4.011	4.015	4.010	4.005	4 009	4.002	4.002	4.011	4.006
30 8	27.8	28.9	31.6	27.9	28.5	33.7	32.5	36.3	32.4	34.6
0.25	0.25	0 27	0.27	0.26	0.27	0.30	0.31	0.31	0.32	0.31

TABLE B2. Electron microprobe data of low-Ca pyroxene.

GSLL4-6 [6]	GSLL4-7 [6]	OLL5-1-1 [4]	OLL5-2-1 [4]	OLL5-3-1 [4]	OLL5-4-1 [4]	OLL5-1-2 [4]	OLL5-2-2 [4]	OLL5-3-2 [4]	OLL5-4-2 [4]	TLL5-1 [4]
55.1 (2)	54.5 (3)	54.6 (1)	54.4 (2)	54.1 (4)	54.6 (1)	54.5 (2)	54.7 (2)	54.7 (2)	54.3 (1)	54.7 (2)
0.07 (7)	0.10 (8)	0 06 (3)	0.16 (8)	0.15 (5)	0 16 (3)	0.16 (7)	0.15 (2)	0.14 (4)	0.19 (6)	0.11 (4)
0 27 (11)	0.26 (14)	0.06 (1)	0.13 (6)	0.47 (67)	0.14 (3)	0.18 (5)	0.15 (3)	0.16 (6)	0.16 (4)	0 09 (4)
0.20 (11)	0.19 (9)	0.08 (2)	0.11 (3)	0.30 (31)	0.09 (2)	0.14 (8)	0.10 (1)	0.09 (4)	0.19 (11)	0.05 (3)
28.5 (2)	28.0 (6)	27.4 (1)	27.2 (1)	27.3 (1)	27.4 (2)	27.2 (2)	27.4 (1)	27.4 (1)	27.3 (1)	27.2 (0)
0.39 (6)	0.52 (21)	0.79 (6)	0.86 (10)	0.86 (17)	0.67 (4)	0.90 (9)	0.74 (8)	0.75 (9)	0.82 (9)	0.71 (4)
0.38 (5)	0.43 (5)	0.43 (2)	0.43 (3)	0.42 (3)	0.43 (0)	0.45 (4)	0.46 (4)	0.44 (3)	0.42 (3)	0.44 (2)
15.0 (3)	15.2 (3)	15.8 (2)	15.7 (1)	15.3 (9)	15.8 (1)	16.0 (1)	15.9 (1)	15.9 (1)	15.9 (3)	16.3 (1)
< 0.03	< 0.03	< 0.03	< 0.03	0.05 (4)	< 0.03	< 0.03	< 0.03	0.03 (2)	< 0 03	< 0.03
99.87	99.20	99.21	98.98	98.96	99.24	99.62	99.65	99.57	99.30	99.59
1.982	1.978	1.989	1 987	1.974	1.987	1.981	1.984	1.985	1.979	1.988
0.002	0.003	0.002	0.005	0.004	0.004	0.005	0 004	0.004	0.005	0.003
0.012	0.011	0.003	0.006	0.020	0.006	0.008	0.007	0.007	0.007	0.004
0.006	0.005	0.002	0.003	0.009	0.003	0.004	0.003	0.003	0.005	0.001
1.527	1.517	1.488	1.479	1.484	1.486	1.476	1.483	1 483	1.482	1.474
0.015	0.020	0.031	0.033	0.034	0.026	0.035	0.029	0.029	0.032	0.028
0.012	0.013	0.014	0.013	0.013	0.013	0.014	0.014	0.014	0.013	0.014
0.452	0.462	0.480	0.479	0.468	0.480	0.488	0.483	0.483	0.485	0.494
0.001	0.001	0.001	0.001	0.004	0.002	0.001	0.001	0.002	0.001	0.001
4.007	4.012	4.008	4.005	4.009	4.006	4.010	4.008	4.008	4.010	4.007
39.3	34.7	35.5	36.8	36.0	36.9	34.8	24.5	25.7	37.3	36.7
0.30	0.30	0.32	0.32	0.32	0.32	0.33	0.33	0.33	0.33	0.34

TABLE B2. Electron microprobe data of low-Ca pyroxene.

TLL5-2 [4]	TLL5-3 [4]	TLL5-4 [4]	SSLL6-1 [4]	SSLL6-2 [4]	SSLL6-3 [4]	SSLL6-4 [4]
54.5 (1)	54 8 (1)	54.7 (2)	55.0 (2)	55.1 (1)	55 1 (1)	55.3 (1)
0.16 (1)	0.11 (6)	0 16 (1)	0 21 (3)	0 23 (0)	0.20 (2)	0 16 (2)
0.12 (2)	0.08 (3)	0.13 (2)	0.17 (1)	0.18 (1)	0.18 (2)	0 16 (1)
0.08 (3)	0.08 (3)	0.09 (5)	0.21 (11)	0.15 (2)	0.11 (4)	0.13 (3)
27.1 (0)	27 3 (1)	27.3 (2)	27.1 (1)	27.2 (2)	27.1 (2)	27.2 (2)
0.78 (8)	0.71 (6)	0.70 (7)	0 93 (8)	0.85 (5)	0.90 (11)	0.84 (7)
0.47 (1)	0.45 (2)	0 45(1)	0.45 (4)	0.45 (1)	0.44 (2)	0.43 (3)
16.5 (1)	16.3 (2)	16.4(7)	15 9 (2)	15.8 (1)	15 7 (1)	15.8 (1)
< 0.03	< 0.03	< 0.03	< 0.03	< 0.03	< 0.03	< 0.03
99 74	99.89	99.90	99.92	100.04	99.76	100.04
1.982	1 986	1.984	1.989	1 990	1 994	1.994
0.004	0.003	0.005	0 006	0.006	0.005	0.005
0.005	0.004	0.006	0.007	0.008	0.007	0.007
0.002	0.002	0.003	0 006	0 004	0 003	0.004
1.469	1.478	1.474	1.460	1.464	1.461	1.465
0.030	0.028	0.027	0.036	0.033	0.035	0.032
0.015	0.014	0.014	0.014	0.014	0.013	0.013
0.502	0.494	0.496	0.480	0.477	0.477	0.477
0.001	0.001	0.001	0.001	0.002	0.001	0.002
4.010	4.008	4 008	3.999	3.998	3 997	3.998
34.6	36.1	36.1	35 1	34.6	35.4	36.7
0.34	0 33	0.34	0.33	0.33	0.33	0.33

TABLE B3. Electron microprobe data of diopside.

Diopside	BML4-1 [6]	BML4-2 [4]	BML4-3 [3]	BML4-4 [4]	HL5-1 [7]	HL5-2 [2]	HL5-3 [2]	HL5-4 [2]	GL6-1 [6]	GL6-2 [6]
SiO_2	53 9 (3)	54.0 (0)	54.2 (2)	53 5 (4)	53.6 (4)	53 7 (4)	54.0 (3)	54 0 (3)	54.0 (1)	53 8 (1)
TiO_2	0.36 (6)	0.39 (5)	0.29 (3)	0.29 (8)	0.33 (5)	0.40 (6)	0.21 (2)	0.23 (2)	0 46 (1)	0 47 (3)
Al_2O_3	0.55 (18)	0.51 (16)	0.36 (4)	0.72 (3)	0 43 (8)	0 48 (14)	0 46 (2)	0 48 (20)	0 50 (2)	0.51 (2)
Cr_2O_3	1.03 (19)	1.09 (20)	0.79 (7)	1.80 (34)	0 74 (16)	0 82 (2)	0 81 (5)	0 83 (8)	0.81 (6)	0 86 (3)
MgO	17.9 (13)	17.0 (3)	17 1 (1)	18 5 (3)	17.1 (7)	16 7 (4)	16 7 (1)	16 7 (1)	16 6 (1)	16 5 (1)
CaO	19.8 (13)	21.4 (10)	22.7 (1)	16.7 (6)	21.7 (8)	22.3 (5)	22 3 (8)	22 2 (0)	21 9 (2)	21.6 (2)
MnO	0.29 (6)	0.25 (6)	0.23 (3)	0 42 (13)	0 21 (3)	0 22 (1)	0.18 (2)	0 20 (1)	0 22 (2)	0.23 (3)
FeO	4.74 (11)	4.10 (57)	3 97 (7)	6.40 (82)	4 37 (3)	4.14 (14)	4 09 (0)	4.16 (13)	4.80 (16)	4.92 (16)
Na_2O	0.59 (9)	0.68 (9)	0.53 (4)	0.78 (3)	0.52 (7)	0 60 (3)	0 55 (3)	0.56 (5)	0 55 (2)	0.57 (2)
Total	99.18	98.95	100.19	99.12	98.98	99.31	99.26	99.39	99.77	99.48
cations based on 6 oxygen										
Si	1.982	1.978	1.981	1 973	1.981	1.979	1 988	1.987	1.982	1 981
Ti	0.010	0.011	0.008	0 008	0.009	0 011	0.006	0.007	0 013	0 013
Al	0 024	0.022	0.016	0 031	0.019	0.021	0 020	0.021	0.022	0.022
Cr	0 030	0.032	0 023	0 053	0.022	0.024	0.024	0.025	0 024	0 025
Mg	0.982	0.937	0 931	1.017	0.939	0.918	0.918	0.917	0 906	0.909
Ca	0.779	0.846	0.887	0 658	0.861	0.879	0.879	0.876	0.863	0.853
Mn	0.009	0 008	0.007	0.013	0.007	0.007	0.006	0.006	0 007	0 007
Fe	0.146	0.127	0.121	0.198	0 135	0.128	0 126	0.128	0.148	0.152
Na	0.042	0.049	0.038	0.056	0 037	0.043	0.039	0.040	0.039	0.041
Total	4.003	4.009	4.011	4.006	4.009	4 009	4.005	4.005	4.002	4.002
Fe/Mn	16.5	17.2	16 8	15.5	20.3	18.2	22.9	21.3	21.8	21.5
Fe/Mg	0.15	0.14	0.13	0 19	0.14	0.14	0.14	0.14	0 16	0.17

TABLE B3. Electron microprobe data of diopside.

GL6-3 [5]	GL6-4 [6]	GWLL4-1 [5]	GWLL4-2 [3]	GWLL4-3 [5]	GWLL4-4 [4]	OLL5-1-1 [4]	OLL5-2-1 [3]	OLL5-3-1 [4]	OLL5-4-1 [5]	TLL5-1 [4]
54.0 (1)	53.9 (2)	52.6 (5)	53.8 (2)	53.2 (5)	53.2 (5)	54.0 (1)	53.4 (1)	53 3 (2)	53.6 (3)	53.8 (3)
0.46 (3)	0.45 (3)	0.41 (12)	0.33 (1)	0.47 (9)	0.46 (13)	0.39 (2)	0.36 (0)	0 32 (1)	0.44 (11)	0.36(0)
0.49 (2)	0.47 (3)	1.71 (35)	0.41 (4)	1.01 (52)	0.76 (36)	0.46 (1)	0.43 (1)	0.45 (5)	0.53 (17)	0.40 (3)
0.71 (4)	0.77 (8)	1.20 (54)	0.68 (1)	1.07 (28)	0.98 (27)	0.73 (5)	0.67 6)	0.69 (5)	0.69 (14)	0.66 (7)
16.7 (2)	16.6 (2)	19.0 (15)	16.4 (1)	15 9 (4)	16.1 (3)	16.3 (1)	16.2 (5)	16.1 (1)	16.9 (8)	16.3 (2)
22.0 (4)	22.1 (1)	15.8 (26)	22.0 (1)	22.0 (21)	22.0 (3)	21.7 (0)	21.4 (2)	21.6 (1)	21.2 (9)	21.7 (5)
0.23 (1)	0.25 (4)	0.29 (4)	0.23 (0)	0.25 (3)	0.20 (2)	0.21 (1)	0.21 (2)	0.22 (2)	0.23 (4)	0.20 (4)
4.54 (27)	4.65 (10)	7.87 (1.5)	4.94 (16)	4 58 (10)	4.57 (22)	5.66 (10)	5.57 (11)	5.66 (17)	5.73 (41)	5.64 (41)
0.53 (3)	0 53 (3)	0.40 (10)	0.50 (2)	0 57 (7)	0.51 (5)	0.51 (1)	0.50 (2)	0.48 (1)	0.48 (5)	0.45 (1)
99.60	99.71	99.26	99.28	99.07	98.86	99.92	98.77	98.71	99 76	99.58
1.984	1.981	1.941	1.986	1.969	1.974	1.985	1.987	1.984	1.975	1 987
0.012	0.012	0.011	0.009	0.013	0.013	0.011	0 010	0.009	0.012	0 010
0.021	0.020	0.075	0.018	0.044	0.033	0.020	0.019	0.020	0.023	0.017
0.021	0.022	0.035	0.020	0.031	0.029	0.021	0.020	0.020	0.020	0.019
0.912	0.912	1.043	0.902	0.879	0.893	0.895	0.898	0.893	0.925	0.897
0.867	0.869	0.623	0 872	0.874	0.875	0.854	0.852	0.860	0.835	0.859
0.007	0.008	0.009	0.007	0.008	0.006	0.007	0 007	0.007	0.007	0.006
0.139	0.143	0.243	0.153	0.142	0.142	0.174	0.173	0.176	0.177	0.174
0.037	0.038	0.029	0.036	0.041	0.037	0.036	0.036	0.035	0.034	0.032
4.001	4.004	4.008	4.004	4.001	4.001	4.002	4.002	4.005	4.008	4.001
19 9	19.0	26.3	21.8	17.9	23.2	26.9	26.1	25.4	25 8	29 0
0.15	0.16	0.23	0.17	0.16	0.16	0.19	0.19	0.20	0.19	0.19

TABLE B3. Electron microprobe data of diopside.

TLL5-2 [4]	TLL5-3 [4]	TLL5-4 [4]	SSL6-1 [6]	SSL6-2 [6]	SSL6-3 [6]	SSL6-4 [6]
53.7 (1)	53.7 (1)	53.7 (7)	53.2 (1)	53 1 (1)	53.1 (3)	53.5 (2)
0.37 (1)	0.37 (2)	0.32 (1)	0.44 (2)	0.43 (1)	0.42 (2)	0.43 (2)
0.42 (1)	0.41 (2)	0 38 (1)	0.49 (2)	0.50 (2)	0.49 (2)	0.49 (1)
0.75 (9)	0.67 (10)	0.68 (3)	0.80 (6)	0.78 (3)	0.76 (4)	0 80 (5)
16.1 (1)	16.2 (0)	16.1 (5)	16.1 (1)	16.1 (0)	16.0 (1)	16.0 (1)
21.8 (1)	22.2 (3)	22.2 (2)	21.2 (1)	21.3 (2)	21.7 (2)	21.4 (2)
0.21 (3)	0 21 (4)	0.16 (2)	0.22 (4)	0.23 (3)	0.23 (3)	0.24 (2)
5.81 (8)	5.20 (22)	5.59 (23)	6.07 (17)	6.05 (14)	5.64 (10)	6.34 (14)
0 50 (2)	0.46 (3)	0.45 (1)	0.51 (2)	0.51 (1)	0.50 (1)	0.54 (1)
99.66	99.38	99.59	98.94	99.09	98.80	99.68
1.982	1.984	1.983	1.979	1 976	1.978	1.978
0.010	0.010	0.009	0.012	0.012	0.012	0.012
0.018	0.018	0.017	0.021	0.022	0.021	0.021
0.022	0.020	0.020	0.023	0.023	0.022	0.024
0.887	0.894	0.889	0.893	0.894	0.888	0.884
0.865	0.878	0.879	0 843	0.850	0.867	0.847
0 007	0.007	0.005	0.007	0.007	0.007	0.008
0.180	0.161	0.173	0.189	0.188	0.176	0.196
0.036	0.033	0.032	0.037	0.037	0.036	0.039
4.006	4.004	4.007	4.004	4.008	4.007	4.008
27.7	23.8	32.9	28.0	27.2	25.0	26.3
0.20	0.18	0.19	0.21	0.21	0.20	0.22

VITA

Heather Kaye Gastineau was born in Indianapolis, Indiana, on May 9, 1976. She graduated from Brownsburg High School in May of 1994 and entered Ball State University in August of 1994 as a music major with primary interest as a flautist. The spring semester of 1995 she was enrolled in Physical Geology and it was then that Dr. Jeffrey Grigsby sparked her enthusiasm in the Geosciences. She was awarded a Bachelor of Science degree in Geology in July of 1998. In the fall of that year, Heather entered the graduate program in Geological Sciences at the University of Tennessee. In August of 2000, she received her Master of Science degree in geology.

Heather accepted an instructor position at the University of Southern Indiana in Evansville, IN to begin in August, 2000, teaching Physical Geology labs and lecture courses.